UPPSALA
UNIVERSITET

Digital Comprehensive Summaries of Uppsala Dissertations from the Faculty of Science and Technology 246

Template-Based fabrication of Nanostructured Materials

ANDERS JOHANSSON

ACTA
UNIVERSITATIS
UPSALIENSIS
UPPSALA
2006

ISSN 1651-6214
ISBN 91-554-6738-5
urn:nbn:se:uu:diva-7364

Dissertation presented at Uppsala University to be publicly examined in Häggsalen, Ångströmlaboratoriet, Lägerhyddsvägen 1, Uppsala, Friday, December 15, 2006 at 13:30 for the degree of Doctor of Philosophy. The examination will be conducted in English.

Abstract
Johansson, A. 2006. Template-Based fabrication of Nanostructured Materials. Acta Universitatis Upsaliensis. *Digital Comprehensive Summaries of Uppsala Dissertations from the Faculty of Science and Technology* 246. 57 pp. Uppsala. ISBN 91-554-6738-5.

Materials prepared on the nanoscale often exhibit many different properties compared to the same materials in their bulk-state. Interest in nanostructured materials has increased because of these properties in fields such as microelectronics, catalysis, optics and sensors. This increased interest in nanostructured materials calls for new and more precise fabrication techniques.

This thesis describes how to use the porous anodic aluminium oxide as a template for the fabrication of a variety of nanostructured materials. Palladium and copper nanoparticles were deposited along the pore walls in anodic aluminum oxide using electroless deposition and atomic layer deposition. In both cases, it was possible to control the size of the nanoparticles by carefully monitoring the deposition parameters. The thesis also describes how Prussian blue nanoparticles and nanotubes can be fabricated using the anodic aluminium oxide as a template. The deposition of Prussian blue was performed by a sequential wet-chemical method. By using atomic layer deposition, it was also possible to deposit thin films of amorphous Nb2O5 on the pore walls. When the template was removed by etching, freestanding nanotubes were obtained. The anodic aluminium oxide membrane was also used as a mask for high energy (MeV) ion irradiation of an underlying substrate. The tracks produced were etched away with hydrogen fluoride. In this way, it was possible to transfer the highly ordered porous pattern from the mask onto other oxides such as SiO2 and TiO2.

All fabricated structures were characterized using a variety of analysis techniques: scanning electron microscopy for evaluating sample morphology; transmission electron microscopy for better resolved investigations of the morphology; X-ray diffraction to assess crystallinity; energy dispersive spectroscopy and X-ray fluorescence spectroscopy to determine the elemental composition and identify possible contaminants.

The general aim of the work described in this thesis has been to create a set of tools for use in the fabrication of a variety of nanostructured materials, whose dimensions composition can be tailored by selecting appropriate fabrication methods and parameters.

Keywords: Nanoparticles, nanotubes, anodic aluminium oxide, electroless deposition, ALD, Nb2O5, Prussian blue, palladium, copper, ion beam lithography, TiO2, SiO2

Anders Johansson, Department of Materials Chemistry, Box 538, Uppsala University, SE-75121 Uppsala, Sweden

ISSN 1651-6214
ISBN 91-554-6738-5
urn:nbn:se:uu:diva-7364 (http://urn.kb.se/resolve?urn=urn:nbn:se:uu:diva-7364)

List of Papers

This thesis is based on the following papers, which are referred to in the text by their Roman numerals.

I. Alenka Razpet, Göran Possnert, Anders Johansson, Anders Hallén and Klas Hjort: Ion transmission and characterization of ordered nanoporous alumina. *Nuclear Instruments and Methods in Physics Research B 222, 593-600 (2004)*

II. Anders Johansson, Jun Lu, Jan-Otto Carlsson and Mats Boman: Deposition of palladium nanoparticles on the pore walls of anodic alumina using sequential electroless deposition. *Journal of Applied Physics 96, 5189-5194 (2004)*

III. Anders Johansson, Erika Widenkvist, Jun Lu, Mats Boman and Ulf Jansson: Fabrication of High-Aspect-Ratio Prussian blue Nanotubes Using a Porous Alumina Template. *Nano Letters 5, 1603-1606 (2005)*

IV. Anders Johansson, Tobias Törndahl, Mikael Ottosson, Mats Boman and Jan-Otto Carlsson: Copper nanoparticles deposited inside the pores of anodized aluminium oxide using atomic layer deposition. *Materials Science and Engineering C 23, 823-826 (2003)*

V. Mårten Rooth, Anders Johansson, Mats Boman and Anders Hårsta: Ordered and parallel niobium oxide nano-tubes fabricated using Atomic Layer Deposition in anodic alumina templates. *Materials Research Society. Symposium Proceeding Volume 901E, 0901Ra24-05.1 (2006)*

VI. Alenka Razpet, Anders Johansson, Göran Possnert, Marek Skupinski, Anders Hallén and Klas Hjort: Fabrication of high-density ordered nanoarrays in silicon dioxide by MeV ion track lithography. *Journal of Applied Physics 97, 044310 (2005)*

VII. Ruy Sanz, Anders Johansson, Marek Skupinski, Jens Jensen, Göran Possnert, Mats Boman, Manuel Vázquez and Klas Hjort: Fabrication of Well-Ordered High-Aspect-Ratio Nanopore Arrays in TiO_2 Single Crystals. *Nano Letters 6, 1065-1068 (2006)*

The Author's Contribution to Appended Papers

I. Half the planning. Half the experimental work. Significant parts of the writing.

II. All the planning. All the experimental parts. All the writing.

III. Major part of the planning. Half the experimental parts. Major parts of the writing.

IV. Half the planning. Half the experimental parts. Major parts of the writing.

V. Half the planning. Half the experimental parts. Half the writing.

VI. Half the planning. Half the experimental parts. Significant parts of the writing.

VII. Half the planning. Significant parts of the experiments. Major parts of the writing.

Abbreviations

AAO	Anodic Aluminium Oxide
ALD	Atomic Layer Deposition
CVD	Chemical Vapour Deposition
EDS	Energy Dispersive Spectroscopy
PB	Prussian Blue
RBS	Rutherford Backscattering Spectroscopy
SEM	Scanning Electron Microscopy
SERS	Surface Enhanced Raman Spectroscopy
TEM	Transmission Electron Microscopy
XRD	X-ray Diffraction
XRFS	X-ray Fluorescence Spectroscopy

Contents

1. Introduction

Nanotechnology is usually referred to as the technology and study of objects in the size range of ~1-100 nm. Mankind has benefited from the field of nanotechnology a long time. The Lycurgus cup [1], dated to the fourth century AD, is crafted from glass containing gold and silver alloyed nanoparticles implanted into it by mistake. The nanoparticles give rise to the color-shifting observed in the cup when comparing light reflected on the cup (green) and light transmitted through the cup (red). At that time the scholar might have called it "magic" but today such phenomenon is explained by Mie theory [2-4] and effective medium theory [5-7].

Nano-sized objects show a great variety of interesting properties and this is the main driving force of the research in the field of nano-technology today. Metal nanoparticles are already widely used for catalysis [8-9]; recent research also suggests that certain noble metal nanoparticles can be used in the fabrications of sensors, since it has been shown that they enhance the number of Raman scattered photons by a factor of $\sim 10^6$ during Raman spectroscopy analysis [10-12]. Yet another driving force for research in the field of nanotechnology is the ongoing miniaturization of electronics. It is increasingly important to understand how small objects behave when the components are decreasing in size. In silica the leakage current increases when the thickness and width of electronic components decreases. As a result other oxide materials have to replace silica with new ways to fabricate these materials. In some cases it might be interesting to have the tools for deposition of thin films on substrates that have a non-planar geometry. A number of nanoporous materials are known today [13] and they offer a palette of interesting substrates for template based fabrication of nanostructures.

In the present thesis, a number of routes for fabrication of nano-objects are described. The basis on the research presented here is the anodic aluminium oxide (AAO) membrane. The membranes are manufactured by oxidation of aluminum under very controlled conditions. AAO membranes are thereafter used for synthesis of:

a. Immobilized palladium, copper and Prussian blue nanoparticles along the pore walls of AAO membranes [II, III, IV].
b. Nanotubes of niobium oxide and Prussian blue, using the AAO membrane as template [V].
c. Patterned SiO_2 and TiO_2 surfaces by using the AAO membrane as a mask in ion beam lithography [VI, VII].

Fabrication of monodisperse nanostructures are of great interest for a variety of applications, since most of the expected properties are size dependent.

The most famous nanotubular system is by far the one based on carbon and the synthesis of carbon nanotubes, first described by Iijima [14] in *Nature* in 1991. In order to obtain ordered nanotubular systems in other materials, a variety of methods have been used. C_{60} on surfaces has been used as growth promotors for synthesis of MoS_2 and WS_2 nanotubes [15]. A common approach to achieve ordered arrays of nano-tubes is the usage of a well-ordered porous material as template for thin film deposition.
AAO provides a template with all pores ordered in parallel and with an extremely small size deviation. The pores are ordered in a hexagonal pattern. By using the AAO membrane as template for synthesis of nanotubes it is possible to obtain monodisperse nanostructures in all kind of materials. This has been thoroughly investigated for nano-rod deposition, using electrochemical methods [16-18], but little is described about depositing along the pore walls, creating nanotubes.

The first part of the thesis summarizes the technique of anodizing aluminum to porous alumina membranes and characterization of the formed membranes [I]; some aspects of electroless deposition [II, III], Atomic Layer Deposition[IV, V] and ion beam lithography [VI, VII]. In the following sections, the experimental setups and methods are described followed by important results which are briefly explained. Finally, the most important findings in this work are summarized.

1.1 Anodization

Anodization of aluminum is a technique which has been used for several decades. During anodization a layer of porous alumina is formed on the surface. This alumina layer is considerably thicker than the native oxide, always present on the aluminum surface, naturally protecting the aluminum from corrosion. By exposing the porous alumina to dyes, it is possible to trap the dyes in the pores, resulting in decorative colors. In the early 90-th researchers started to develop techniques for anodization under more controlled conditions [19-22] in order to produce porous alumina with monodisperse pore diameters ordered in a perfect hexagonal pattern. The most cited reference among the first papers in the field is probably Masuda *et al.* in Science 1995 [19]; that paper describes how to produce AAO membranes with perfectly parallel pores, ordered hexagonally using a two step anodization technique (see Figure 1.1).

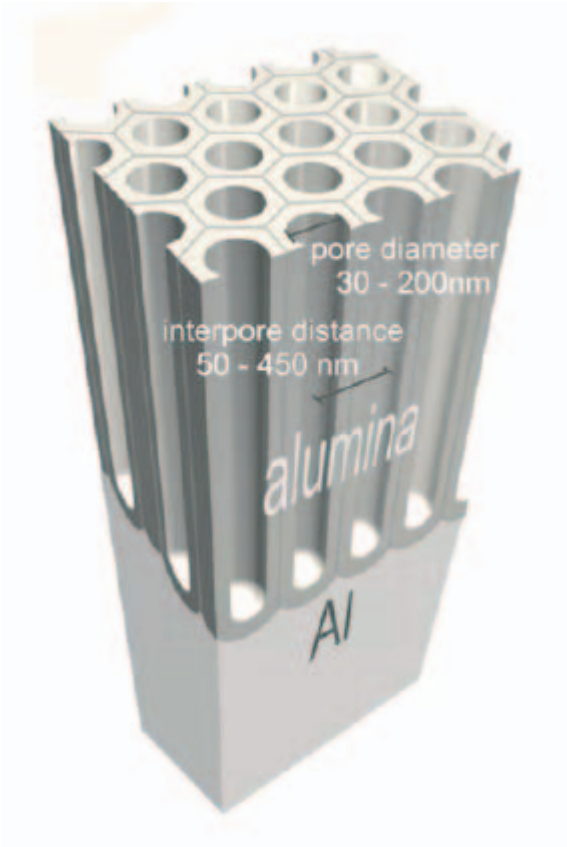

Figure 1.1. Schematic image of the AAO membrane.

The high ordering of the pores, which is possible to obtain by choosing appropriate electrolyte and film-forming conditions, is unique for the aluminum system. In order to obtain hexagonally ordered porous alumina membranes it is necessary to anodize in an electrolyte which promote the dissolution of the formed alumina film [22]. Such electrolytes can consist of *e.g.* sulphoric acid, phosphoric acid or oxalic acid. When applying a constant voltage anodically over an aluminum substrate, an oxide layer starts to form rapidly. The oxide forms in the Al/Al_2O_3 interface due to the transport of O^{2-} /OH^- through the alumina film. At the same time, the oxide forms in the Al_2O_3/electrolyte interface because of Al^{3+} ions migrating outwards in the film [20]. While the oxide is formed another competing process is going on; namely a dissolvation of the formed alumina film. Partly the dissolvation occurs because of the electrolytes dissolving alumina. The Al-O bonds are also polarized by the electric field present over the oxide film, normal to the aluminum surface, and this polarization enhance the dissolvation of the oxide. The electrical field is higher where the oxide film is thin. A higher elec-

tric field promotes more dissolvation of the oxide, leading to formation of pores in the alumina film. The located dissolvation of alumina together with the build-up of new oxide results in the formation of a porous structure.

It is also important to perform the anodization under fairly low temperatures (typically 1 ºC). Low anodization temperature gives a considerably lower formation rate of the porous alumina, which is necessary for the system to relax mechanically, *i.e.* order the pores hexagonally.

The pores are getting ordered form the bottom and up in the anodization process. To get them completely ordered all through the membrane it is necessary to introduce a pre-arranged pattern before anodization. Masuda *et al.* [19] suggested that the anodization should be carried out in two steps. After one long anodization (~24 h) the formed alumina is stripped away. This creates a hollow pattern in the aluminum. After stripping**,** another anodization is performed. This time the pores start to form in the hollow pattern from the previous anodization, ordering the pores from bottom to top. The pre-patterning can also be done using a mold and lithographic method**s** [23-27]. In this way it is possible to obtain a long-range ordering of the porous structure. If not the molding technique is used, domains (several μm^2 in size) with perfect order will exist, but between them there will be "grain boundaries". In Figure 1.2 some of the boundaries between ordered areas are highlighted.

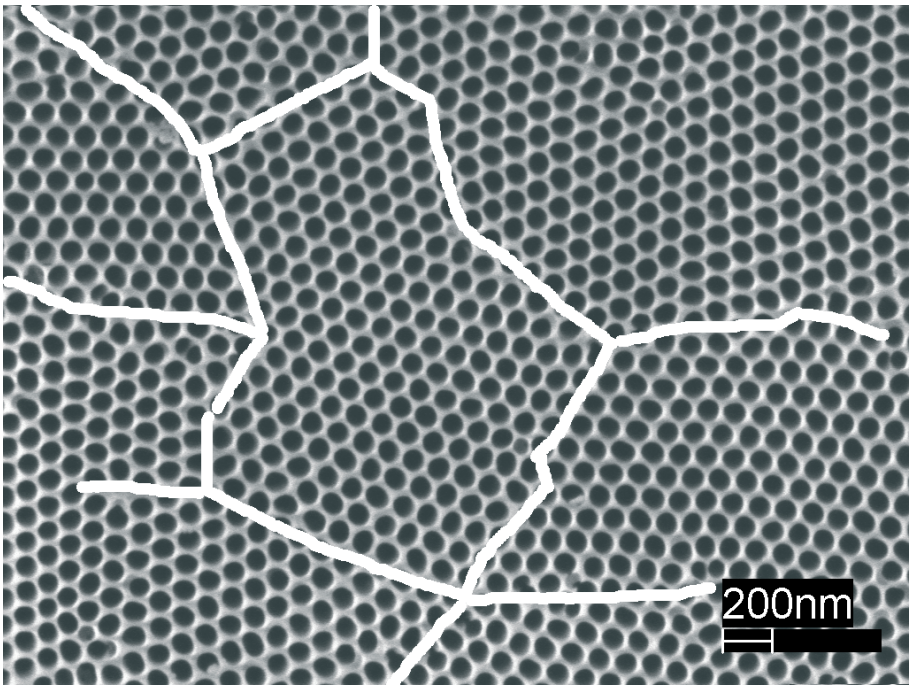

Figure 1.2. SEM images in which some of the "grain boundaries" between the ordered domains in AAO have been highlighted.

There are several ways to characterize the anodic alumina membranes. Most important are probably electron microscopy and spectroscopical methods, both in the visible and the X-ray region. This is described by Thompson *et al.* [20]. In this thesis an alternative route is presented for characterization of the anodic alumina membrane. By irradiating the membranes in transmission mode with MeV ions the parallelity, as well as the size of the pores, can be determined [I].

By controlling the voltage during anodization it is possible to monitor the inter-pore distance as well as the pore diameters [16-22]. The thickness of the membranes can be tailored by controlling the time for the second anodization. It is difficult to produce membranes thicker than ~100 μm due to dielectric breakdown of the formed alumina. It is, however, possible to produce much thicker AAO membranes by utilizing so called *hard anodization*, recently described by Lee *et al* [28].

1.2 Liquid based deposition in porous alumina

1.2.1 Electrodeposition

The possibility to fill the pores of porous anodic alumina using standard electrodeposition techniques has been studied since the middle of the 90-th. A great number of conductive materials have been deposited inside the pores of anodic alumina; mainly for the purpose of studying magnetic behavior in the nano-scale (a review was written by Sellmyer *et al* [29]). Recent studies [30] have also shown that it is possible to deposit nanotubes using electrochemical methods. The technique makes use of electroless deposited silver nanoparticles along the pore walls, which make nucleation more favorable on the pore walls. By a careful control of the electrolyte concentration and the current density it is possible to deposit the material as thin films on the pore walls. Usually, the material will deposit as filled rods from the bottom of the pores and out to the electrolyte. Electrodeposition in porous anodic alumina has not been studied in this thesis.

1.2.2 Electroless deposition

To make use of the large surface of the anodic alumina substrates, it is interesting to deposit other materials on the pore walls, and thereby tune the

surface properties of the porous membrane. By using electrodeposition, most commonly deposition results in a complete filling of the pores. To fabricate nanotubes by using the AAO as template it is necessary to selectively deposit the material only on the pore walls. To deposit metal nanoparticles along the pore walls a variety of techniques have been utilized [31-35]. In most cases the nanoparticles are synthesized "outside" the AAO template and in a subsequent stage introduced and bonded to the pore walls by chemical or physical techniques. Noble metal nanoparticles deposited along the pore walls of anodic alumina may be of great interest for Surface Enhanced Raman Scattering (SERS) applications [12], as well as for catalysis. In this thesis a method to attach size-tailored palladium nanoparticles along the pore walls of AAO is presented [II]. The deposited palladium nanoparticles can be used as nucleation sites for selective deposition of other materials.

Prussian blue is another interesting material to deposit inside the pores of AAO. Prussian blue and many of its analogues shows a great number of fascinating magnetic properties [36-39]. The cobalt analogue to Prussian blue, cobalt hexacyano ferrate, is a novel optomagnetic material which can be switched from diamagnetic to paramagnetic and *vice versa* by applying light of a proper wavelength [40-41]. Both Prussian blue and its cobalt analogue have been fabricated earlier by using a sequential wet deposition technique [42-44]. Prussian blue has also been electrodeposited inside the pores of AAO, both as rods and as tubes [36, 37, 45]. In this thesis a manufacturing method of Prussian blue nanotubes is presented. The present technique is based on sequential deposition and the use of AAO as templates [III].

1.3 Atomic Layer Deposition

Most of the deposition techniques used today can produce thin films of good quality but are unable to produce conformal films of accurate thickness on 3-D substrates, thus excluding the possibility to fabricate template based nano-structures. Especially techniques based on physical vapor deposition such as evaporation and sputtering have poor step coverage. Atomic Layer Deposition, ALD, on the other hand offers several advantages over such techniques since ALD is able not only to produce thin films of excellent quality but also has an unsurpassed conformality and accurate thickness control over large areas. This makes ALD a natural choice as a deposition technique on complex 3-D substrates such as AAO. The ALD technique was developed by Suntola and Antson in the 1970's [46] and have since then been widely examined.

ALD is a pulsed version of chemical vapor deposition (CVD). One precursor gas at a time is introduced to the substrate. In between the precursor pulses the substrate is purged with an inert gas, *e. g.* argon or nitrogen to remove unadsorbed precursors and by-products. The adsorbed precursors

react under controlled temperature to produce a monolayer of the desired reaction product in a self-limiting process. The pulses are then repeated until a desired thickness of the deposited film is reached. The principle is demonstrated in Figure 1.3.

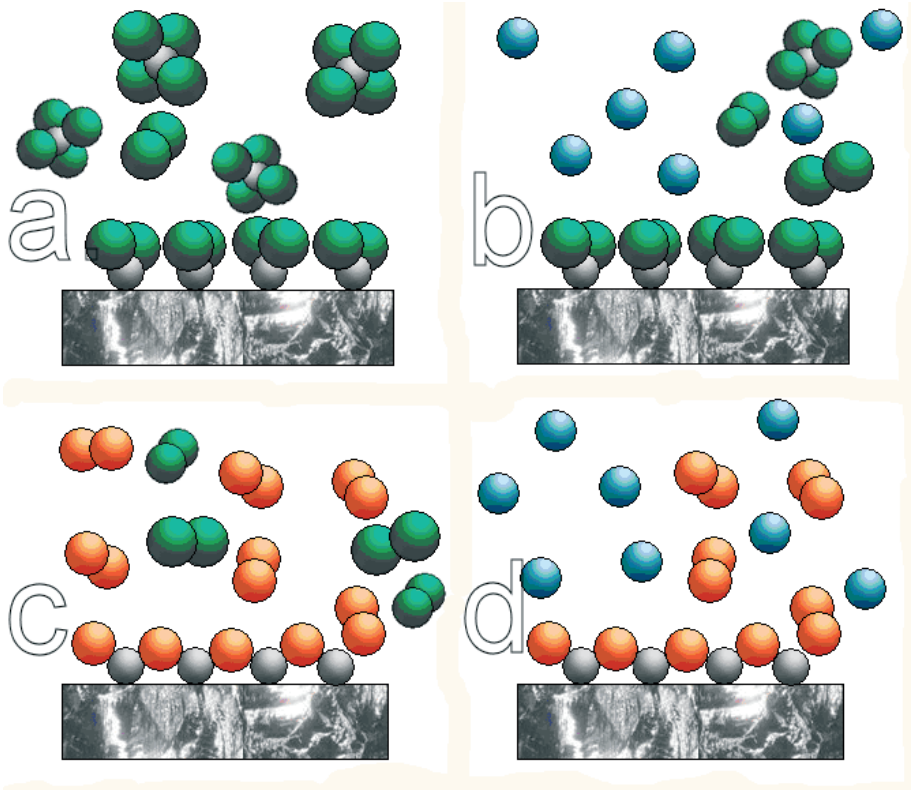

Figure 1.3. Schematic description of ALD. a. precursor 1 is adsorbed to the substrate. b. excess of precursor 1 is purged. c. precursor 2 is introduced and reacts with adsorbed precursor 1. d. by-products and excess of precursor 2 are purged.

1.3.1 Metal deposition using ALD

Depositing metal thin films on oxide substrates using ALD can be problematic. This is mostly due to poor nucleation and/or weak adhesion of the metals on the substrates. Copper is an interesting material to deposit on oxide substrates due to its numerous applications in the field of electronics. Recently a number of groups have suggested how to deposit copper and copper containing materials using ALD [47-50]. The method described by Törndahl *et al.* [49] describes how copper can be deposited on oxide sub-

strates. By using the same method, nanoparticles have been deposited along the pore walls of AAO membranes [IV]. Here again the excellent step-coverage of ALD is utilized, resulting in an even coverage of copper nanoparticles along the pore walls in AAO.

1.3.2 Metal oxide deposition using ALD

Metal oxides have been deposited on planar and 3-D substrates using a variety of precursors, most of which are summarized by Puuranen in a review from 2005 [51]. Common for deposition of metal oxides using ALD, are metal halide precursors, especially metal chlorides; but the use of organometallic precursors is also widely spread, both in ALD and CVD [52]. In the work using ALD described here, mainly metal iodide precursors were used [54-58].

In this thesis the focus has been to perform depositions in deep-trench structures [59, 60]; in the pores of AAO [V]. No other deposition technique today offers the advantages of a precise tuning of the film thickness when deposition in trenches with aspect-ratios (width over depth) of up to 1000-2000. However, it is important to significantly increase the pulse lengths compared to depositing on planar substrates. In the in-house built reactor used for these studies the most utilized pulse length is four seconds when depositing on planar substrates. When 3-D substrates such as AAO were used, the typical pulse length was 30 seconds.

1.4 Ion beam lithography using AAO as mask

Ion beam lithography has been used for patterning of materials for many years [61, 62]. The basis of ion track lithography is the inelastic energy transfer from swift heavy ions to the atoms in the lattice of the bombarded materials via ionization and excitation. If the energy loss exceeds a certain threshold, a noncontinuous latent track is formed in the irradiated material, forming a string-of-pearls line of transformed material. At a higher threshold the string-of-pearls become a continuous latent track, which can be developed into a pore after selective chemical etching [63]. Compared to low-energy (keV) ion beam lithography [64-66], where elastic scattering in dominating, the lateral scattering of high-energy (MeV) ion track lithography is minute. Even if low-energy ion beams can be used to transfer a pattern from a mask it is difficult to get good aspect-ratios due to the large scattering of the ion beam when the energy increases, up to the threshold for formation of latent ion tracks[66].

A continuous ion track shows the highest contrasts known in lithography, with aspect-ratios of hundreds and above. Each track created by an incident ion is developed into a cylindrical pore. However, fabrication of nanostructures should also be possible when the energy loss of an incident ion is only above the threshold of track formation, if high ion fluences are applied and sufficient overlapping of the transformed material is created in the irradiated volume. Additionally, heavy ions enable such high-energy transfer on radiation hard materials like amorphous SiO_2 which can be transformed and developed lithographically.

AAO membranes offer a unique array of pores. However, the anodization technique for obtaining porous alumina is only applicable for the aluminum system. One way to get the same patterning in other materials can be to deposit a material covering the alumina changing only the surface properties of AAO, as described in sections 1.2 and 1.3 in this thesis. If the bulk properties of another material should be studied and there is still a need for a perfect porous pattern, a transfer of the pattern from the alumina must be performed to another material. This can be of interest when studying photonic crystals [67]. If a thin mask of alumina is mounted on a surface of another material as a mask, the AAO pattern can be transferred by irradiating the sample with a MeV ion beam.

The pores in the in-house made AAO's are extremely parallel, which have been shown in a publication included in this thesis [I]. However, a careful alignment of the AAO membrane with respect to the incident ion beam is necessary. The alignment was done by using a thin (< 10 nm) gold layer between the substrate and the mask and the RBS signal from gold was maximized by moving the sample.

1.4.1 Patterning of SiO_2 using AAO as mask

There are several ways to create pores in Si and SiO_2. Most techniques are based on traditional keV lithography, but by using these techniques it can be challenging to reach the "nano-scale". The last couple of years the interest of transfer the porous pattern of AAO to silicon oxide has increased; *e.g.,* within the field of high density memory structures, a direct patterning of SiO_2 would be desirable. There are reports of pattern transfer using chemical etching methods [68] and ion beam lithography using keV energies [66]. The method described here is based on MeV ion beam lithography, where an AAO mask is mounted on a silicon substrate which has been oxidized on the surface to amorphous SiO_2 [VI].

1.4.2 Patterning of TiO_2 using AAO as mask

TiO_2 has the highest known dielectric constant of the oxide materials. This property gives TiO_2 suitable characteristics in electronic and optic applications; *e.g.,* it was suggested that titanium oxide (rutile) would be a good gate oxide for the next generation of MOSFET (for review see [69]). This is due to the low electric tunneling of titania at the nanometer scale. Additionally, crystalline TiO_2 has interesting properties as a catalyst in some chemical reactions. Recent work demonstrates that the surface of crystalline nanoporous TiO_2 can be used for photocleavage of water [70]. In this thesis a method for high aspect-ratio patterning of TiO_2 single crystals by means of ion beam lithography is demonstrated [VII].

2. Experimental

2.1 Anodization

In this study two types of AAO's have been used; commercial available AAO's, sold as filter membranes (Anodisc 13) by Whatman Ltd. and in-house anodized AAO's; typically with a pore width of 60 nm and an inter-pore distance of 100 nm. The thicknesses of the AAO's were typically 2 nm but other thicknesses were commonly made too.

For in-house fabrication of AAO it is necessary to use as well polished aluminum substrates as possible. Aluminum plates were bought from Good-fellow, and were pre-polished to a smoothness of 1 Ra or better. The pre-polished substrates were electropolished in an electrolyte consisting of 1:4 by volume of perchloric acid (65%) and ethanol (99.5%). The voltage was set constant to 20 V and the electropolishing were performed for three minutes at a constant temperature of 1 ºC. The electropolishing results in a mirror like surface on the aluminum. The anodization is then performed in two steps in order to reach a good ordering of the pores [19]. The first step is an anodization in oxalic acid (0.3 M). The polished alumina substrate is mounted as anode and an inert lead electrode as cathode. Anodization is performed under a constant potential of 40 V and rigorous stirring; the electrolyte is kept at a temperature of 1 ºC. The setup is shown in Figure 2.1.

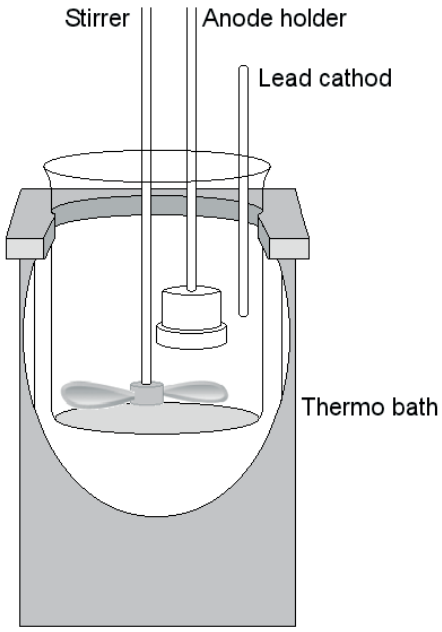

Figure 2.1. Schematic setup for anodization.

After the first anodization the formed alumina film is etched in a stripping solution containing chromic acid (1.8 wt-%) and phosphoric acid (6 wt-%). After stripping a patterned aluminum surface is left [19]. The pattern formed is used as template or mold for the second anodization. A second anodization is initialized using the same anodization parameters as in the first anodization step. However, the oxide thickness can be tailored by controlling the time for the second anodization step. The thickness of the formed film has a linear correlation with the anodization time during the first five hours, typically 0.5 μm/h, using these parameters.

After the second anodization it is convenient to open the pores, since the pore diameter is usually < 25 nm. The pores are opened in a 4.25 wt-% phosphoric acid solution. 90 minutes of pore-opening in the given solution gives pores with a diameter of about 60 nm. However, it is difficult to control the pore diameter by carefully monitoring of the pore-opening time. This is probably due to different ageing of the formed oxide, a process which is not completely understood. Parameters that might be involved are the moisture of the air in the laboratory as well as the temperature and the quality of the chemicals.

In order to achieve an aluminum-free alumina membrane it is necessary to selectively etch the aluminum prior to pore-opening. The etching can be performed in a number of solutions. One way is to use a saturated $HgCl_2$-solution and thereby produce an amalgam, which easily can be removed from the free membrane. Another way is to expose the aluminum side to an oxidizing $CuCl_2$/HCl-solution, where copper is formed under a redox reaction in which aluminum is oxidized. Using the last approach gives an opportunity to mask the aluminum and just open the aluminum bottom partially.

To investigate the parallelity of the pores in the AAO membranes a 2 MeV He^+ beam, collimated to a spot with a diameter of ~2 mm^2, were used. The beam current on the sample were measured to 2 nA. Three thicknesses were investigated; 2, 7 and 10 μm and the pore diameters were 70 nm with an inter-pore distance of 100 nm. The membranes were mounted to a sample wheel which could be tilted and rotated in all directions. The ion transmission was measured indirectly by counting the number of ions backscattered from a gold target behind the sample wheel. The reason for this was that the transmitted high ion current could damage the detector if the beam were allowed to directly hit the detector. An additional detector was mounted in a conventional RBS setup at the scattering angle of 168º to obtain additional information about the AAO membrane.

2.2 Electroless deposition

2.2.1 Deposition of metal nanoparticles

Immobilized palladium nanoparticles were deposited on the pore walls of AAO's. The AAO's used for these synthesis were commercially available membranes from Whatman Ltd. Particles were deposited from $\{Pd(NH_3)_4\}^{2+}$ solutions with concentrations ranging from 0.01 M to 0.5 M. The solutions were prepared from palladium (II) chloride (99.9%, Aldrich) and ammonia. Ammonia was added in excess in order to drive the equilibrium to favor the palladium ammonia complex - $\{Pd(NH_3)_4\}^{2+}$

The deposition system used consists of a temperature controlled hot-air gun and a cylindrical aluminum sample holder with a hole in it (see Figure 2.2). The temperature of the air-flow was varied between 100 and 500 ºC with a flow of 500 L/min. During the depositions the AAO membrane was placed on the holder and a droplet (~0.05 ml) of the deposition solution was applied to the membrane. The heater was pre-heated to the desired temperature and at the same time the solution wetted the AAO membrane with help of the capillary forces. The heater was placed 15 mm over the sample holder and the solution soaked AAO membrane was heated for 15 s. The AAO membrane was thereafter cleaned in de-ionized water in ten portions of 2 ml.

After cleaning the AAO membrane was dried in an air-flow with a temperature not exceeding 100 ºC for about 20 s.

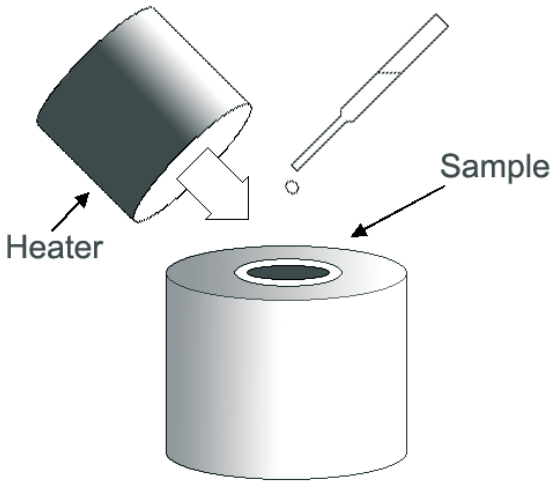

Figure 2.2. Set-up for deposition of palladium nanoparticles.

2.2.2 Sequential deposition of Prussian blue

Both commercially available AAO membranes and in-house made membranes were used as templates in this study. The in-house fabricated AAO membranes used were 5 µm in thickness with pores of ~60 nm in diameter. The inter-pore distance (centre to centre) was 100 nm.

Three solutions were prepared for the depositions:

1. 0.20 M KCl, 0.01 M $K_4[Fe(CN)_6] \cdot 3H_2O$, pH adjusted to 3 using HCl (aq).
2. 0.20 M KCl, 0.01 M M $FeCl_3 \cdot 6H_2O$, pH adjusted to 3 using KOH (aq).
3. Buffer solution with 0.20 M KCl, pH adjusted to 3 using HCl (aq)

For the depositions the membranes were placed in Solution 1 for 15 min, after which it was cleaned in Solution 3 for 15 minutes. The membranes were then dipped in Solution 2 for 15 minutes and thereafter recleaned in Solution 3. This procedure, called a deposition cycle, was repeated until the desired amount of PB was deposited. The number of deposition cycles was varied between 1 and 10. The dipping procedure involved careful stirring with a magnetic stirrer, and Solution 3 was renewed between each step.

A nucleation enhancer for PB deposition in order to achieve a continuous film on the pore walls was deposited using the technique described earlier (see section 2.2.1).

After the deposition of PB nanotubes in the AAO template the alumina could be selectively etched away in a 4.25% H_3PO_4 solution; leaving the PB as free-standing nanotubes.

2.3 Atomic Layer Deposition

The depositions using ALD presented in this thesis were performed in two similar reactors in-house built. A brief description of the reactors will be given here.

The principles for ALD are given in Figure 3. The figure gives an overview over the synthesis of a binary metal containing compound and involves four pulses. In the first pulse the metal precursor (in the gas phase), is introduced to the deposition zone. The second pulse injects a purging gas (typically N_2 or Ar), which purge the remains of the precursor and leaving only a monolayer of the metal containing molecules on the surface. In the third pulse the second precursor is added. The second precursor reacts with the first precursor to form the desired product. Finally purging gas is introduced again in the fourth pulse to remove excess of the second precursor and the formed by-products. The pulse lengths are typically a few seconds, when depositing on flat substrates. However, depositing in 3-D substrates like AAO templates requires much longer pulse times in order to saturate the surfaces. Throughout the studies described in this thesis typical pulse lengths of 30 s were used. The mentioned pulse-scheme will be denoted a *cycle*. The thickness of the deposited films can be tailored by repeating the cycle until the desired film thickness is achieved.

The reactors (see Figure 2.3) used for the ALD are both of the flow type hot wall reactors using quartz tubes. Quartz allows for deposition at higher temperatures than normally employed in ALD – up to about 1050 °C. Both the reactors have three independently controlled temperature zones. The gas pulses are controlled by pneumatic valves, opened and closed by means of computer control. In all processes described in this thesis, solid metal halide precursors were sublimated and introduced into the reaction zone.

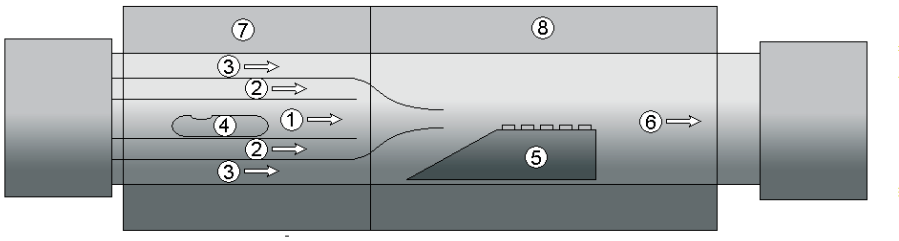

Figure 2.3. The ALD reactors used in these studies. The reactor consists of the following parts: 1. Carrier gas for solid precursor. 2. Purge gas, bulk flow. 3. Reactant gas. 4. Container for solid precursor. 5. Substrate holder. 6. Outlet of gases to pump. 7. Furnace for evaporation of solid precursor. 8. Furnace for heating of reaction chamber.

2.3.1 Copper deposition

Copper nanoparticles were deposited using CuCl as the copper precursor. The different gases that were employed in the different pulses are presented in Table 2.1.

Table 2.1. Pulse sequence scheme used for ALD of copper nanoparticles

Pulse	Gas
1	Ar + CuCl(g)
2	Ar (purging gas)
3	H_2O
4	H_2O/H_2
5	H_2
6	Ar (purging gas)

The pulse lengths were varied between 10 and 30 s. For most of the depositions the following pulse lengths were chosen: 30 s for CuCl, 15 s for water, 15 seconds for the combined water/hydrogen pulse and 15 s for hydrogen. The purging pulses were all 30 s. The process parameters are summarized in Table 2.2.

Table 2.2. Process parameters for copper nanoparticles deposition using ALD

Parameter	Value
H_2	100 sccm
H_2O	2.5 mg/pulse
CuCl	0.3 – 0.4 mg/pulse
Ar	250 sccm
Linear flow	1.1 m/s
Total pressure	8 Torr
Deposition temperature	425 ºC
CuCl evaporation temperature	340 ºC
Number of cycles	100, 200, 400 and 800

2.3.2 Metal oxide deposition

For metal oxide deposition mainly metal iodides were used as precursors, except for the deposition of Fe_2O_3 where the metallocene was used instead. Throughout the depositions all pulse lengths were set to 30 s. In Table 2.3. the process parameters are summarized for ALD of Nb_2O_5.

Table 2.3. Process parameters for deposition of Nb_2O_5 using ALD.

Parameter	Value
O_2 (partial pressure)	1 Torr
NbI_5	3 mg/pulse
Linear flow rate	1 m/s
Total pressure	2 Torr
Deposition temperature	475 ºC
NbI_5 evaporation temperature	320 ºC
Number of cycles	150

After ALD of Nb_2O_5 in the pores of AAO, CVD of Nb_2O_5 was performed, using the same precursors and the same reactor for 5 hours. With CVD, which has lower step coverage than ALD, the exposed side, i.e. the side facing the gas phase, of the alumina template was covered with Nb_2O_5, thus blocking the pores completely.

To archive free-standing nanotubes it is necessary to remove the AAO template. This was done by using the technique shown in Figure 2.4. The remaining aluminum on the back side is then etched in a $CuCl_2$/HCl solution; and the AAO template is etched in 4.25% H_3PO_4. However, when Fe_2O_3 was

deposited, NaOH had to be used for etching of the AAO template instead since the phosphoric acid also etches Fe_2O_3.

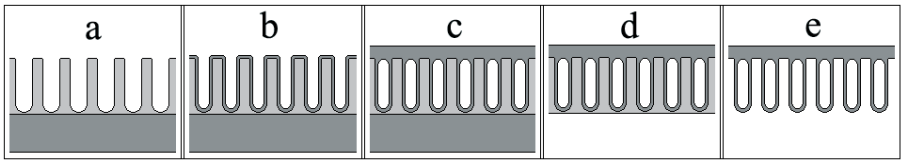

Figure 2.4. Schematic description of the experimental technique to achieve free-standing nanotubes.

2.4 Ion Beam lithography

AAO masks with a thickness of 2 μm were prepared as described earlier in 2.1. The remaining aluminum was completely removed by exposing it to a saturated $HgCl_2$ solution. The AAO masks were pore-opened in phosphoric acid and cleaned in deionized water. The substrates to which the pattern from the AAO mask should be transferred to were carefully cleaned. Prior to attachment of the AAO mask, a thin layer (<10 nm) of gold was sputtered on the substrate. The AAO masks were placed on the substrates and left to dry. When the substrates were dry they were in direct contact with the underlying substrates.

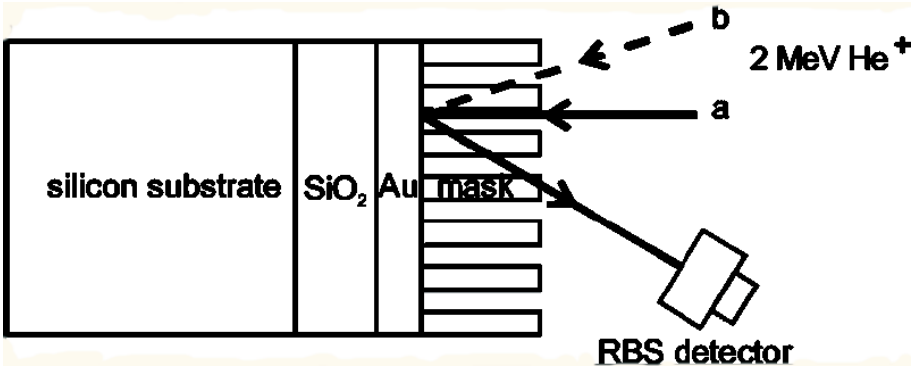

Figure 2.5. Alignment of the mask with respect to the beam using RBS. An ion passing through the membrane as in the b path will loose more energy than an ion passing in path a.

In order to transfer the pattern of the AAO mask to the underlying substrate, by means of ion beam lithography, a careful alignment procedure is necessary. The AAO masks are 2 μm thick and the pores are about 70 nm.

That gives a calculated acceptance angle of 3.6º. In order to align the pores with respect to the incoming ion beam, RBS spectra (2 MeV He^+) from the samples were taken from a variety of angles (see Figure 2.5). The number of He^+ ions backscattered from gold in a selected energy interval was recorded at different sample orientations. An ion passing exactly through a pore is expecting to have higher energy after scattering compared to an ion passing the solid material on the outgoing path (see Figure 2.6). The sample orientation, which had the greatest number of counts in the selected energy interval, was chosen for ion beam lithography.

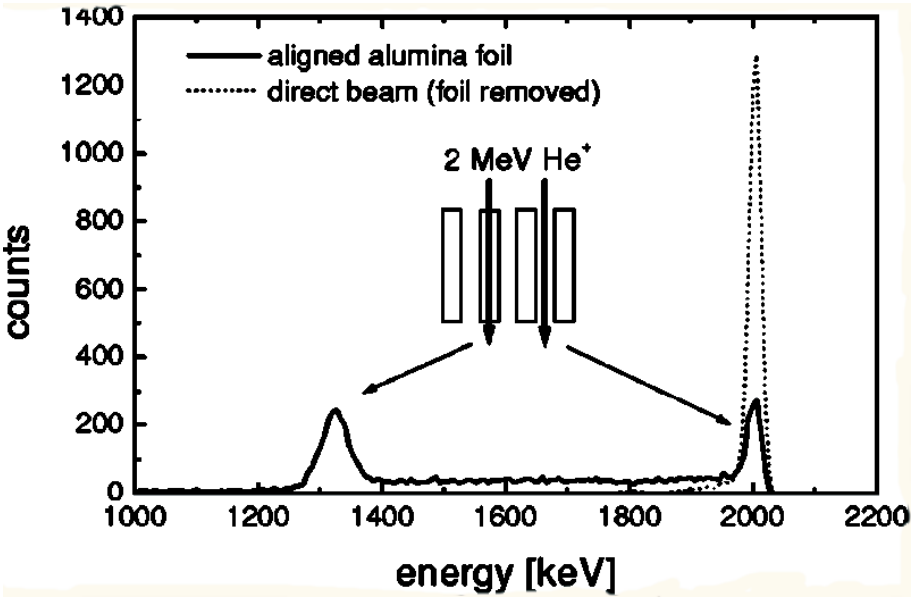

Figure 2.6. Transmission spectrum of ions passing through the AAO mask, through the pores and through the pore walls.

After alignment the samples were irradiated with heavier ions. Two types of substrates were irradiated, thermally grown SiO_2 on silicon and single crystal TiO_2 (rutile). After irradiation the masks were mechanically removed and the samples were etched in HF. Simulations were performed by a computer program - SRIM200317, to estimate the depth of the ion tracks.

2.5 Characterization

The deposited nano-structures and nanoparticles were characterized with respect to their microstructure, morphology, size distribution, thickness and chemical composition with the analysis techniques described below. The

materials which were patterned using ion beam lithography were analyzed with respect to their morphology and microstructure. Table 2.4 gives an overview of the different analysis techniques used for characterization in the papers included in this thesis. The table also summarizes the main information obtained using the techniques.

Table 2.4. Analysis for characterization in the present thesis.

Technique	**Information**	**Paper**
XRD	Phase content	II – V
XRFS	Impurities	II – V
SEM	Morphology	I – VII
TEM	Morphology, film thickness, elemental composition	II, III, V
Raman	Phase content	VII

Grazing incidence XRD was used under an incident angle of 5º to determine the crystal structure of the deposited materials. The incident angle was optimized in order to maximize the analyzing volume and the intensity.

XRFS was used to examine the purity of the deposited material with respect to contaminants. The detection limit of the instrument used is below 1 at-% enabling relatively small amounts of contaminants to be detected.

SEM was used as the standard technique for evaluating the morphology of the deposited structures. The SEM used in all the studies has a field emission gun as electron source and for imaging an in-lens detector were used. In order to optimize the resolution when operating the electron microscope on semiconducting materials it is necessary to decrease the acceleration voltage and the working distance. The two parameters were typically set to 3 kV and 2 mm, respectively.

TEM was also used in order to further confirm the data obtained from SEM. The TEM was equipped with an EDS analyzer which was used for obtaining the elemental composition for the deposited structures.

Raman was used to investigate the microstructure of the pattern transferred material. The data were compared with data from non-irradiated samples.

3. Anodization

The pore-size as well as the inter-pore distance and membrane thickness can be varied by tuning the anodization parameters [16-23]. It is often written that the inter-pore distances can be varied arbitrarily between 10 and 500 nm. If anodization is performed using the technique of Masuda *et al.* [19] the statement above is not really true. The pores will not be well ordered in all the inter-pore intervals. The three most common parameters for anodization, which gives rise to an ordered pore-structure, are:

1. 2 M sulfuric acid at a constant voltage of 25 V; gives an inter-pore distance of 30 nm.
2. 0.3 M oxalic acid at a constant voltage of 40 V; gives an inter-pore distance of 100 nm.
3. 0.3 M phosphoric acid at a constant voltage of 195 V; gives an inter-pore distance of 500 nm.

In order to fabricate AAO membranes with a well-ordered hexagonal pore structure it is also important to anodize at low temperatures. All anodizations described in this thesis were performed at a constant temperature of 1 ºC.

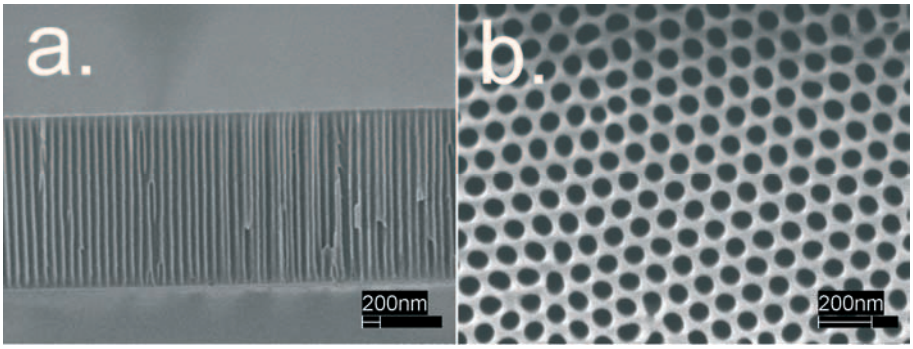

Figure 3.1. SEM images of in-house fabricated AAO membrane from a cross-sectional view (a) and a top-view (b).

Figure 3.1 shows a typical in-house fabricated AAO membrane. In Figure 3.1 a. a cross-sectional image is shown and Figure 3.1 b. shows a top-

view image. In Figure 3.2 a commercial AAO membrane is shown for comparison. It can clearly be seen that the membranes produced in-house have a significant higher degree of order and parallelism than the ones purchased.

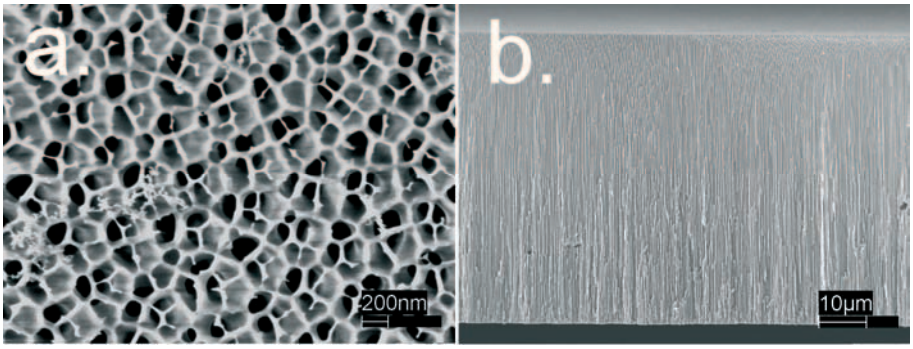

Figure 3.2. SEM images of commercial AAO membrane from a top- view (a) and a cross-sectional view (b).

In order to use the AAO membranes as masks for ions beam lithography it is necessary that the pores are completely parallel. Using the setup described under 2.1 and removing the membrane, the ion beam produced one sharp peak in the spectra. An additional spectrum was taken when an AAO was mounted and aligned with respect to the ion beam (Figure 3.3 a.). One sharp peak can be observed at the same position as was the case when no sample was mounted in the beam path; indicating that a significant part of the beam is transmitted. When misaligning the sample in an azimuth angle of 2º a large number of ions appear at lower energies and the number of directly transmitted ions decreases (Figure 3.3 b.). If the sample is further misaligned to 8 º the sharp peak at no energy loss almost vanishes (Figure 3.3 c.).

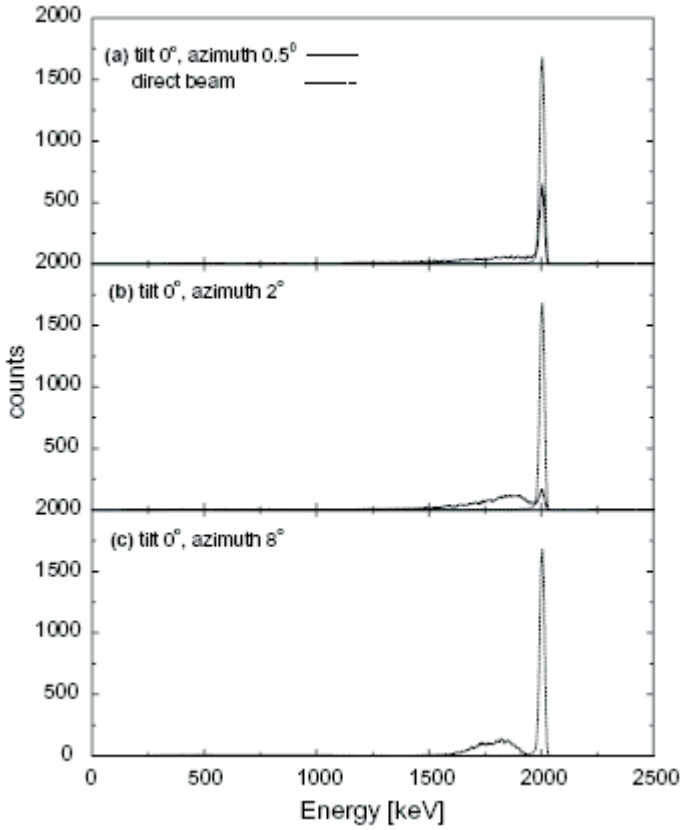

Figure 3.3. Number of ions passing through the membrane at different angles, compared with a direct beam.

The alignment was performed by record the number of counts at an energy interval between 1980 and 2030 keV while changing the orientation of the sample. The angular scans were performed in steps of 0.5º in both the tilt and the azimuth angles. The acquisition time in each position was 15 s. The results for the alignment experiments of the 2 and 7 μm thick samples can be seen in Figure 3.4 a. and b. for the both samples respectively. The ion transmission was defined as the ratio between the transmitted current through the membrane at aligned position and the direct current measured when the sample was removed.

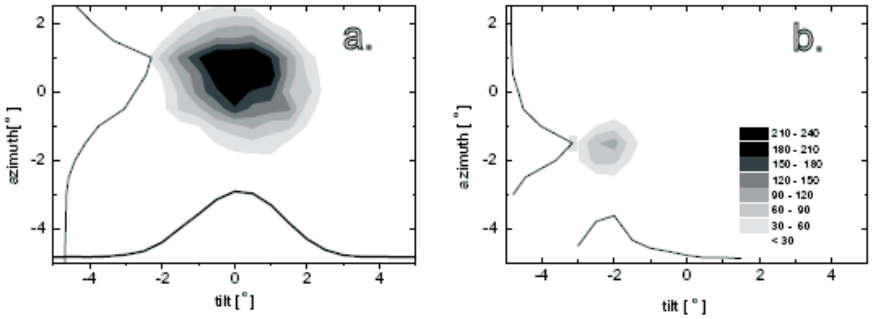

Figure 3.4. 3D histograms of the number of ions passing at different azimuth and tilt angles for a 2 µm thick membrane (a) and a 7 µm thick membrane (b).

In general the thin membranes gave the highest transmission, but differences could be observed for samples with the same thickness and even for pieces fabricated from the same alumina foil. The thin sputtered gold layer did not influence the transmission significantly. Membranes with a thickness of 10 µm were also considered for transmission experiment, but it was never possible to obtain a higher transmission than <1%. For membranes with a thickness of 7 µm, the transmission was ~20%, and for membranes with thicknesses of 2 µm the transmission varied between 30 - 60%.

The same experiment was repeated with O^+ ions, only one peak was seen here as well, indicating that the mask thickness was sufficient to stop the ions not entering a pore.

Observing the SEM images and analyzing the pore percentage on the surfaces of the AAO membranes gives an approximate value of 45%. A transmission of 45% was also observed on some of the 2 µm thick AAO membranes. However, the results showed a dependence on the sample quality, indicating that heavy ion transmission can be a good way to evaluate the quality of the AAO membranes. The fact that the thin membranes gave transmission results comparable to the pore density can be assign to the larger acceptance angle (2º) for the 2 µm membrane compared to the 7 µm membrane with an acceptance angle of 0.6º, *i.e.,* the thicker the membrane, the more difficult to align it with respect to the ion beam.

4. Electroless deposition

A number of deposition techniques have been utilized to deposit nanoparticles along the pore walls in 3-D nanostructures [30, 31]. Most of the techniques synthesize the nanoparticles before introducing them into the porous structure followed by some sort of attachment of the particles to the pore-walls [32-35]. In this thesis a handful of deposition techniques are described. In this chapter the focus is on electroless deposition. But all of the techniques described here are based on deposition of material directly on the pore walls inside the AAO.

4.1 Palladium nanoparticles deposition

It is common knowledge that the platinum metal surfaces show good catalytic activity in various reactions. One drawback in the use of these metals is the high price. By reducing the mass and at the same time increase the surface *i.e.*, fabrication of small particles means that the mass to surface ratio will be lowered. There are a number of techniques for fabrication of palladium nanoparticles; *e.g.,* electroless deposition [71, 72] and laser direct writing [73]. The technique used here is a sequential electroless deposition technique, see 2.2.1.

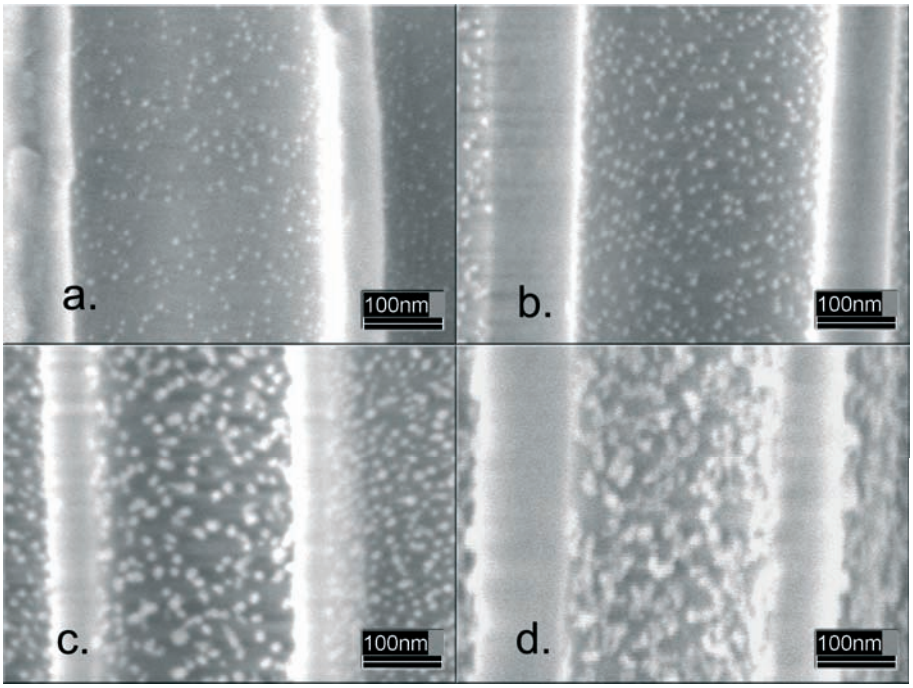

Figure 4.1. SEM images of cross-sectional views of AAO's with Pd nanoparticles deposited on the pore walls, for 3 (a), 10 (b), 20 (c) and 35 (d) deposition cycles.

Some of the sampled produced in this study can be viewed in Figure 4.1. All of the samples were prepared using an air-flow temperature of 500 ºC and a $Pd(NH_3)_4^{2+}$ solution with a concentration of 0.1 M. Figure 4.1 a, b, c and d shows images of samples prepared using different number of deposition cycles; 3, 10, 20 and 35 for the four samples respectively. In Table 4.1 the results from the study can be viewed, *i.e.,* the number of deposition cycles, the air-flow temperature, the concentration of the palladium containing solution, particle mean diameter and the number of particles per area unit.

Table 4.1. Results from Pd deposition using different deposition parameters.

Number of depositions	**Temperature of air-flow**	**$[Pd(NH_3)_4^{2+}]$ (M)**	**Particle mean diameter and standard deviation (nm)**	**Density of particles ($nm^{-2} \times 10^{-3}$)**
1	500	0.1	6.3; 0.7	5.9
3	500	0.1	6.5; 0.8	3.3
5	500	0.1	7.3; 0.9	3.8
10	500	0.1	8.2; 1.0	2.8
15	500	0.1	9.8; 1.3	2.8
20	500	0.1	10.7; 1.8	2.2
23	500	0.1	10.6; 1.7	2.2
25	500	0.1	10.8; 1.5	2.1
35	500	0.1	-	
10	500	0.01	6.0; 0.9	5.0
10	500	0.5	-	
5	400	0.1	7.5; 1.2	2.5

The particle diameters increased linearly with the number of deposition cycles up to ~20, where the particles started to agglomerate. On samples produced using 35 deposition cycles an almost complete coverage of the pore walls could be observed (see Figure 4.1 d.), making estimations of particle diameters impossible. The size distributions can be observed in Figure 4.2 a-c for 3, 10 and 20 deposition cycles respectively. One would expect to see a log-normal trend in the size distributions [74], which is also observed in Figure 4.2 a. and c. However, the distribution shown in Figure 4.2 b deviates from log-normal. On all samples the size distribution is fairly narrow indicating that the method is effective for producing immobilized nanoparticles.

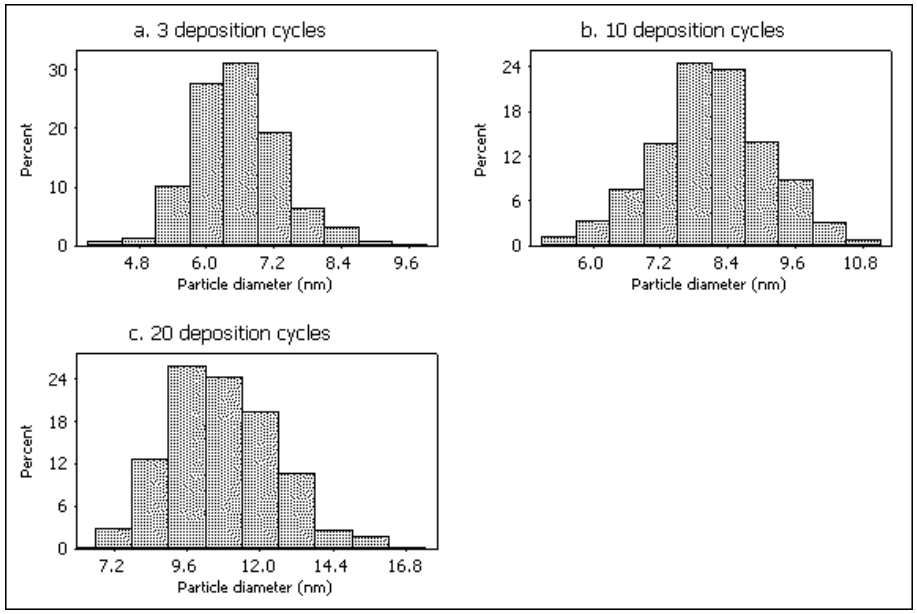

Figure 4.2. Particle size distribution for Pd nanoparticles deposited on the pore walls of AAO's using 3 (a), 10 (b) and 20 (c) deposition cycles.

If the amount of $Pd(NH_3)_4^{2+}$ is the same every time before heating the samples, it would be expected that the mean volume of the particles would increase linearly with the total volume of the nanoparticles produced in the AAO membranes. The particle mean volume was plotted versus the number of depositions; this can be viewed in Figure 4.3.

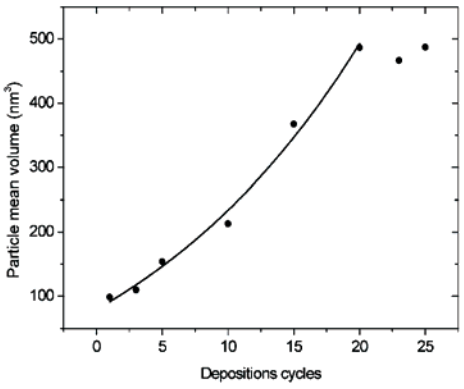

Figure 4.3. The Pd nanoparticle mean volume plotted versus the number of deposition cycles.

As can be seen in the figure the increase in volume is more or less exponentially related to the number of depositions. This could indicate a coa-

lescence of the nanoparticles when the number of depositions increases. This hypothesis is further strengthened by the plateau in the plot when the numbers of deposition cycles are plotted versus the mean particle diameter (Figure 4.4). After ~20 deposition cycles the particles start to form aggregates which upon further depositions form an intact layer on the pore walls.

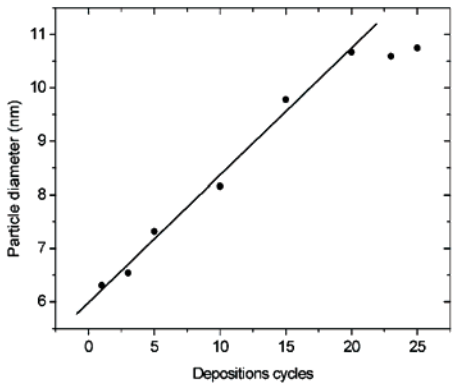

Figure 4.4. The Pd nanoparticle mean diameter plotted versus the number of deposition cycles.

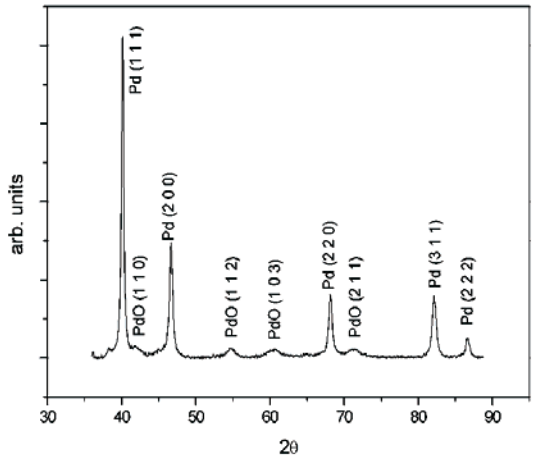

Figure 4.5. X-ray diffractogram of Pd nanoparticles deposited along the pore walls of AAO's. Some PdO can be observed but the samples mainly consists of metallic Pd.

By decreasing the temperature the mean particle diameter decreases slightly as can be seen in Table 4.1. The standard deviation has increased and the particle density has decreased. This indicates that with less thermal

energy available the nucleation process is more favorable on already existing palladium particles. Increasing the concentration of the deposition solution resulted, as could be expected, in a denser deposition of nanoparticles

The microstructure was investigated using XRD and the diffractogram is presented in Figure 4.5. As can be seen in the diffractogram, mainly palladium metal is formed. There are also indications of palladium oxide, PdO, this amount was however low. The reproducibility was investigated using ICP-MS and confirmed to be good.

4.2 Prussian blue deposition

A precipitate of PB is formed instantly by mixing Solution 1 and Solution 2 (see 2.2.2). By applying the two solutions sequentially, and in between them a washing step, to AAO templates it is possible to get self-terminating growth of PB nanoparticles. The chemical reaction involved has been known for decades and can be formulated as:

$4Fe^{3+}(aq) + 3Fe(CN)_6^{4-}(aq) \rightarrow Fe_4[Fe(CN)_6]_3(s)$

The size of the formed nanoparticles could be tailored by varying the number of deposition cycles (see 2.2.2). After a certain number of deposition cycles the particles were large enough to be in contact with each other and thereby create larger aggregates; forming a covering film. By continuing the deposition process the film thickness could be increased.

The particle-size dependence on the number of deposition cycles is demonstrated in the cross-sectional SEM images in Figure 4.6. It can also be seen in figure 4.6 that the PB crystals have a cubic shape.

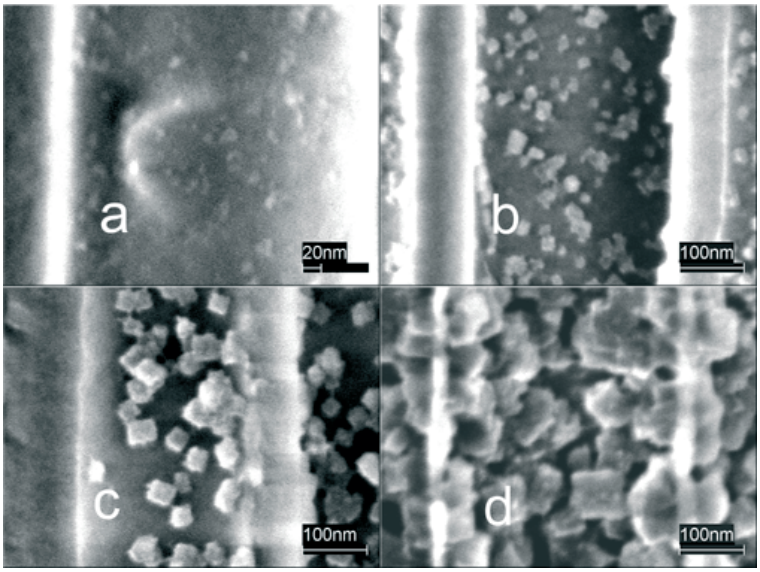

Figure 4.6. SEM images of PB nanoparticles deposited along the pore walls of commercial AAO's using 1 (a), 3 (b), 5 (c) and 10 (d) deposition cycles

By etching the AAO template free PB nanotubes were obtained (see Figure 4.7). The tubular shape of the PB is obvious. However, some pinholes can be observed.

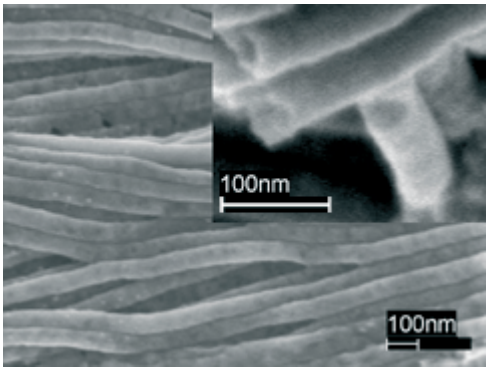

Figure 4.7. SEM image of PB nanotubes after the AAO template was etched away. The insert shows the hollows in the tubes.

The tube wall thickness can be estimated from TEM images. In Figure 4.8, a TEM image of PB nanotubes with a wall thickness of 20 nm is presented.

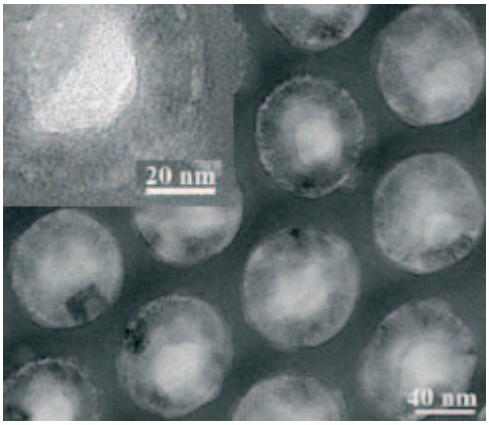

Figure 4.8. TEM image of the Prussian blue nanotubes after four deposition cycles inside the in-house fabricated AAO template; the insert shows the wall thickness of the nanotubes.

When depositing in in-house fabricated alumina membranes it was difficult to obtain tubular systems. This was due to nucleation problems, and the problem was solved by first depositing palladium nanoparticles as nucleation sites. This resulted in a much denser PB deposition, which in turn made fabrication of PB nanotubes with smaller outer diameter possible.

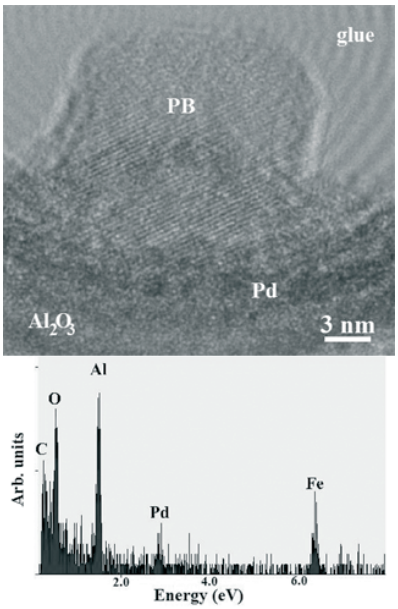

Figure 4.9. TEM image showing (a) the palladium interface between the AAO pore wall an the deposited PB and (b) an EDS spectrum for the sample region shown in a.

EDS (Figure 4.9) confirmed the chemical composition to consist of mainly C, O, Pd and Fe. Nitrogen could not be observed but this is probably due to the peak overlapping with oxygen. XRD showed the deposited PB to have a fcc spacegroup with a = 10.15 Å (Figure 4.10). The background is a result of the amorphous AAO template.

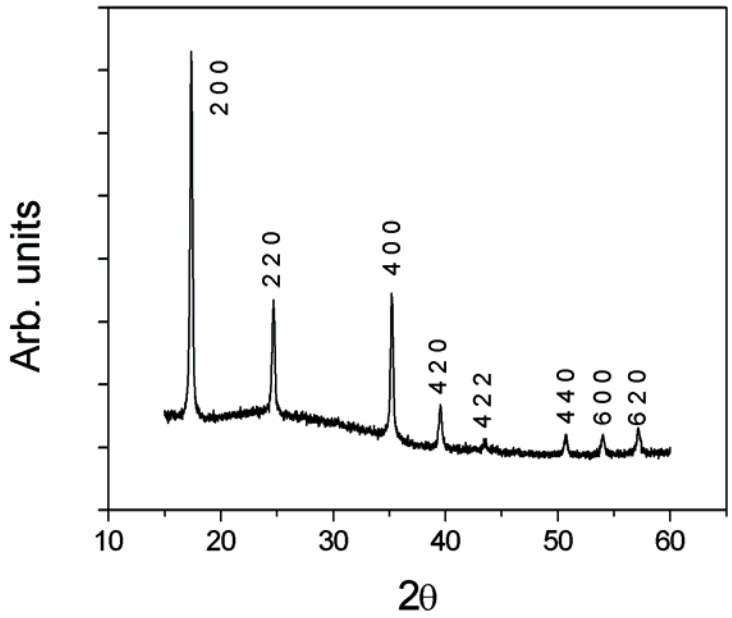

Figure 4.10. X-ray diffractogram showing the fcc crystal structure of the deposited Prussian blue; Cu K_α radiation.

5. Atomic Layer Deposition

5.1 Copper nanoparticles deposition

In the field of microelectronics, copper has obtained much interest recently due to its good conductivity. Copper thin films have been deposited mainly through electrodeposition [75]. The last decade other deposition techniques have been investigated as well. These techniques involve electroless deposition [76], CVD [77-79] and more recently ALD [47-50].

An approach to achieve deposition only on the pore walls can be the use of ALD. This is discussed in this chapter of the thesis.

When depositing copper using ALD it is commonly known that copper grows as islands on oxide substrates. Using the precursor combination and parameters utilized here it is difficult to obtain a continuous film. There are reports describing how to overcome the problem with poor nucleation of copper on oxide substrates. One way is to introduce a seed layers consisting of cobalt [81]. Other approaches are reported, where the authors are using an intermediate step where Cu_3N is formed and later on annealed to achieve metallic copper films.

The process which is described in this thesis for fabrication of copper nanoparticles along the pore walls of AAO is earlier described by Törndahl *et al* [49, 50]. The copper is assumed to be formed via the following two reaction:

$$2CuCl(ad) + H_2O(g) \rightarrow Cu_2O(s) + 2HCl(g)$$

$$Cu_2O(s) + H_2(g) \rightarrow 2Cu(s) + H_2O(g)$$

In the first step the CuCl precursor is introduced to the system and adsorbs to the substrate surface. The system is purged using argon gas, leaving approximately one monolayer of CuCl on the substrates. In the H_2O pulse and the combined H_2O/H_2 pulse the chlorine ligands are interchanged with oxygen from water, forming Cu_2O and HCl. The water is switched of and a pure H_2 pulse is introduced, reducing Cu_2O to Cu. A last argon pulse purges the substrate from by-products. The cycle scheme is repeated.

The experimental parameters used in this study can be viewed in section 2.3.1. When comparing the deposition in AAO membranes with depositing on flat substrates [49, 50] a much higher amount of material is deposited.

This can also be seen when examining XRFS data from samples where AAO membranes have been subjected for copper deposition; about a hundred fold increase of the copper signal is observed. Since the pores in the AAO substrates penetrate completely through the pores, XRFS could also be used to compare the copper content on the two sides of the AAO membranes. If the side facing upwards in the ALD reactor had a higher content of copper, it meant that the deposition had not reached completely through the pores. This can be exemplified by decreasing the time in the precursor pulse to 10 s. In the case with shorter precursor pulse lengths the amount of deposited copper was not equal on both sides of the membrane. The side facied down in the ALD reactor had significantly lower copper content. The same result was obtained when using 10 s purging pulses. When the CuCl pulse and the purging pulses were chosen to 30 s and the H_2O, H_2O/H_2 and H_2 pulses all were chosen to 15 s, the XRFS revealed equal amounts of copper, irrespectively of which side was examined. This indicates that the deposition reached completely through the AAO substrates.

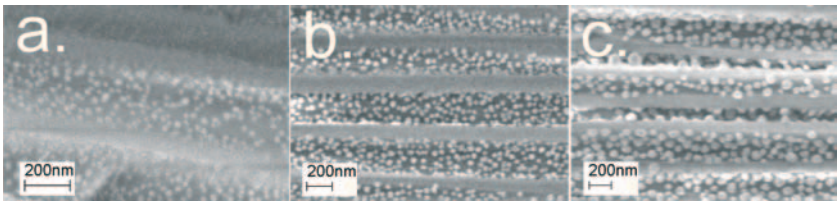

Figure 5.1. Cross-sectional SEM-images of nanoporous alumina substrates where copper nanoparticles has been deposited for 100 cycles (a) 200 cycles (b) and 400 cycles (c).

Figure 5.1 a-c shows cross-sectional images of samples where 100, 200, and 400 deposition cycles have been performed. It can be seen that the size of the formed nanoparticles are increasing with the number of deposition cycles.

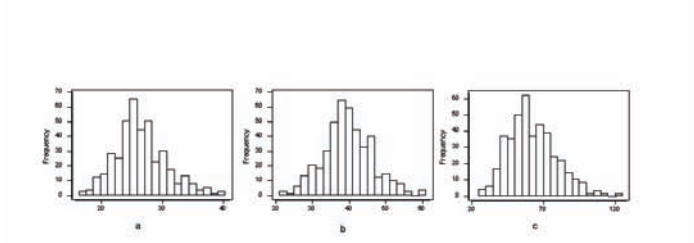

Figure 5.2. Histograms showing the size distribution of copper particles deposited with ALD during 100 (a) 200 (b) and 400 (c) cycles in the pores of nanoporous alumina.

Figure 5.2 a-c shows the size distributions for the same samples. The size distributions are fairly narrow and the copper nanoparticles are not agglomerated. XRD reveals metallic copper but also small amounts of Cu_2O. One possible reason for that might be that not all Cu_2O was reduced in the ALD process. When applying 800 deposition cycles in the ALD process the pores on one side was almost sealed which resulted in a gradient through the AAO membrane.

5.2 Metal oxide deposition

Metal oxides were deposited as films along the pores of AAO using ALD. Process parameters can be viewed in section 2.3.2. In this thesis only the results from the niobium oxide deposition in AAO templates is considered [V].

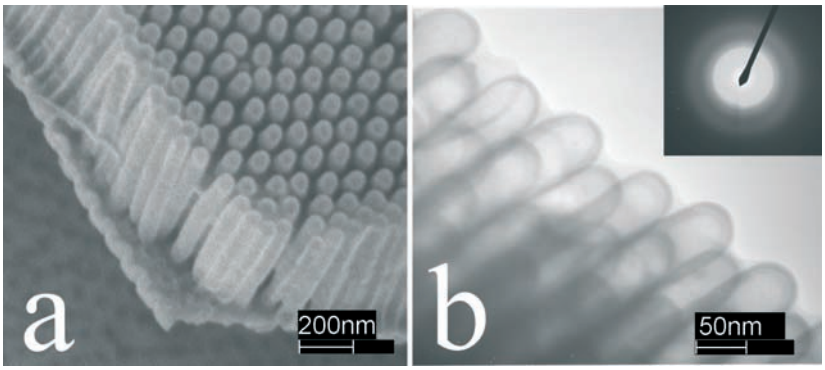

Figure 5.3. SEM image (a) and TEM image (b) showing Nb_2O_5 nanotubes with outer diameters of 60 nm and a wall thickness of 5 nm.

The SEM image in Figure 5.3 a. shows Nb_2O_5 nanotubes deposited using AAO templates with pore diameters of 60 nm. No remaining template can be observed, telling us that the etching time in phosphoric acid was sufficient. It can also be seen in Figure 5.3 a. that the nanotubes remained intact after etching away the template. 150 deposition cycles were used and from the TEM image in Figure 5.3 b. it can be seen that the wall thickness is approximately 5 nm. Furthermore, electron diffraction (insert in Figure 5.3 b.) revealed that the deposited Nb_2O_5 was amorphous, which was expected when depositing at 400 ºC [58].

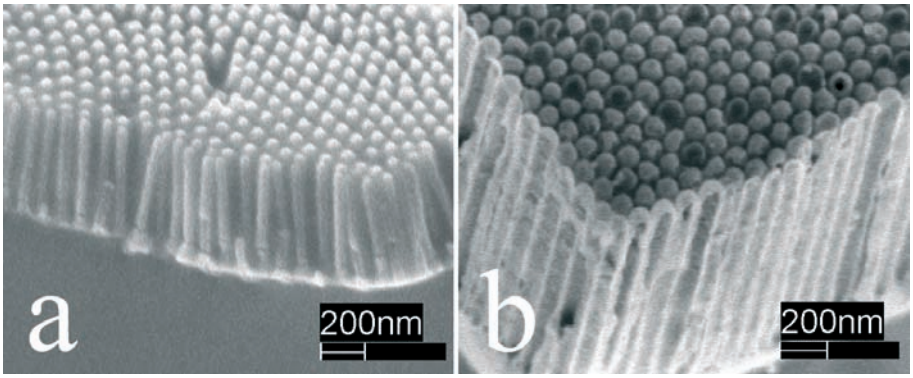

Figure 5.4. SEM images showing Nb_2O_5 nano-tubes with outer diameters of 40 nm (a) and outer diameters of 80 nm (b).

Nb_2O_5 was also deposited in AAO templates with pore diameters of 40 and 80 nm. As can be seen in Figure 5.4, the size of the pores correlates well with the outer diameter of the tubes after etching of the AAO template. All the nanotubes formed in this study were strongly attached to the CVD grown bottom layer of Nb_2O_5. With the nanotubes strongly attached to the bottom, the hexagonal ordering from the AAO template was preserved (see Figure 5.3 a.). The growth rate was the same over the entire pore structure. This indicates that ALD was an excellent technique for tuning the wall thickness of nanotubes, using AAO membranes as templates. The growth rate was slightly lower when depositing on AAO templates (~0.03 nm/cycle) compared to deposition from the same temperature and the same precursors on silicon substrates. The reason for this might be the result of a pressure fall inside the pores which gave a lower partial pressure of O_2. The effect of the O_2 partial pressure on the growth rate is a well known phenomenon in ALD of oxides [82]. Another reason for the lower deposition rate might be the more complex geometry of the substrate.

Other oxides have also been deposited inside AAO templates using ALD. These studies are not included in this thesis.

6. Ion beam lithography

When doing ion beam lithography and using an AAO membrane as mask, the most important part is to get a careful alignment of the pores in the AAO membrane with respect to the ion beam. Since the whole idea is based upon stopping ions hitting the inter-spacing between the pores and let other ions pass through, the alignment is very crucial.

Numeral ideas have been tested for mounting the AAO mask on the substrate which should be patterned. It turned out that the best way to attach the mask to the substrate was to fabricate the mask in the way described in section 2.1. After pore opening in phosphoric acid and cleaning in deionized water, the membrane was placed on the substrate when it still was wet and left to dry there. In this way the AAO mask was attached in direct contact with the underlying substrate, probably due to electrostatic forces. In order to have something to align against it is necessary to have a thin gold layer between the substrate and the AAO mask. The alignment procedure is described in section 2.4. A typical angular scan over the sample during alignment is presented as a two-dimensional histogram in Figure 6.1. The number of counts between channels 260 and 340 in the RBS spectra were scanned both in the tilt and the azimuth angle. An optimum was found and chosen for further ion bombardment.

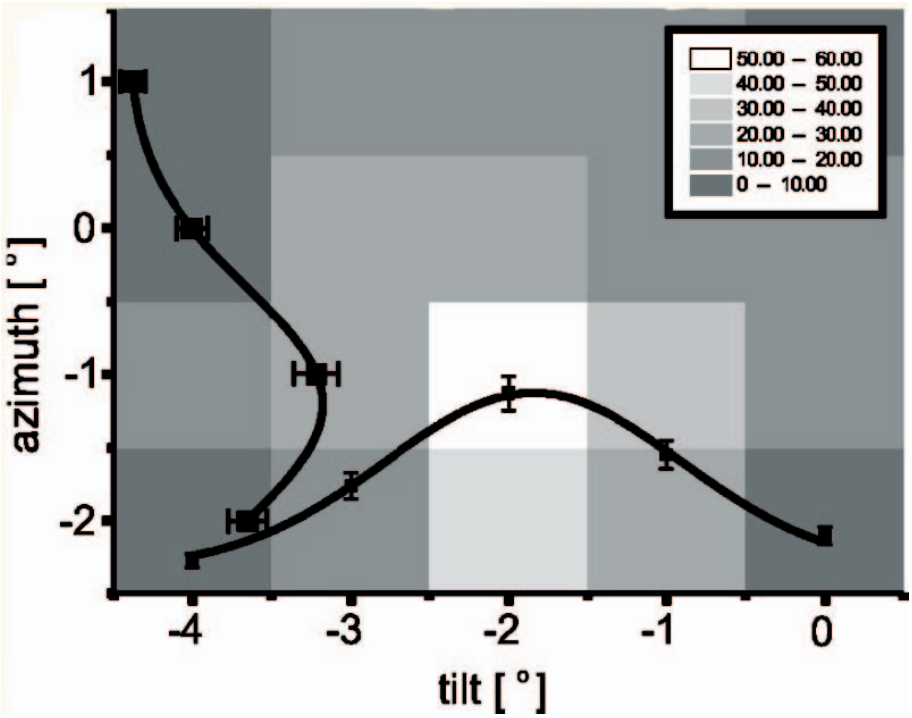

Figure 6.1. 3D histogram of the number of ions passing at different azimuth and tilt angles

A computer program, SRIM200317, was used to simulate the depth to which ions of different energy and mass could reach in the underlying substrate. The energy was chosen so that ions passing the massive parts in the mask would be completely stopped. Yet, the ions have to create as deep tracks as possible in the underlying substrate in order to achieve a high aspect-ratio. If the energy is increased to a level that is too high, etching will occur on locations between the pores as well. This does not increase the aspect-ratio, it rather locate the aspect-ratio maximum using that particular thickness of the membrane.

6.1 Pattern transfer to SiO_2

The AAO membranes used in this study had pore diameters of 30 and 70 nm with an inter-pore spacing of 100 nm. By measuring the ion transmission from membranes prepared, with pore diameters of 30 nm, it was concluded that ~30% of the ions were transmitted without a significant energy loss. This correlates with what would be expected geometrically as calculated from the pore density from these types of membranes.

After irradiation the samples were etched in a HF solution. A pattern transfer could be observed from both types of AAO membranes as can be seen in Figure 6.2. However, the sample which was irradiated through a membrane with 30 nm pores was more sensitive to the placement and orientation of the mask. In Figure 6.2 a. it can be seen that the pores in some areas (i) are somewhat elongated in one direction. That is probably due to a slight misalignment of the mask. In other areas however, the pores are not elongated at all (ii).

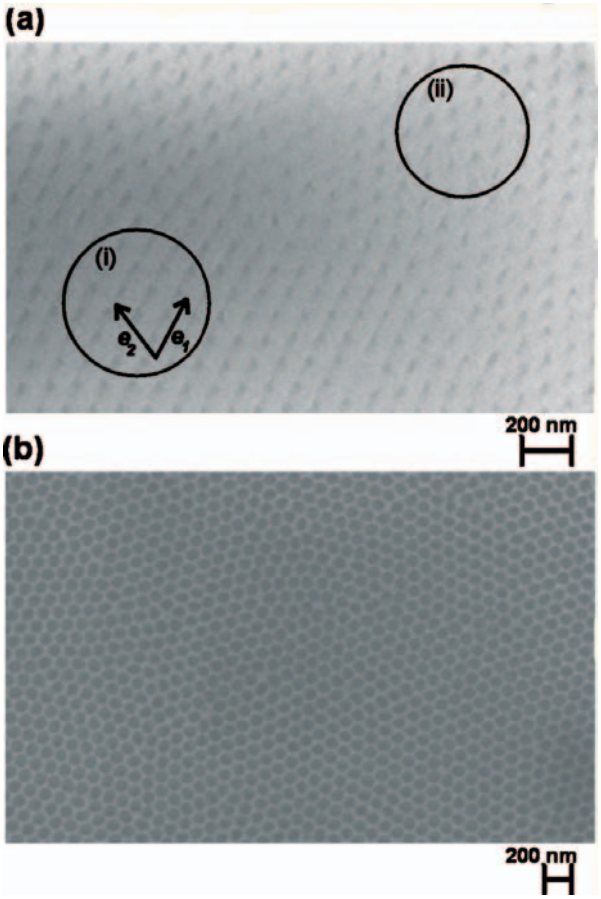

Figure 6.2.(a) SEM image of an irradiated SiO_2 surface 25 s of etching in 5% HF; (i) along the lattice vector e_1 shallow lines can be seen between pores, (ii) lattice appears to be more regular in directions of basic lattice vectors, (b) irradiated SiO_2 surface after 40 s of etching in 5% HF.

Chemical etching produces holes in the irradiated volume only if sufficient damage is introduced to the material. It has been shown earlier [83]

that the enhancement of the etch rate in SiO_2 is correlated to the shift of the infrared absorption frequency peak ω_4 associated with the asymmetric stretch vibration of Si-O bonds. The dependence of ω_4 on the ion dose has been measured for different ions. It was found that for ions heavier than C, the frequency decreased and reached its saturated value at doses below 10^{15} cm^{-2}. This is in agreement with our studies; showing that no etchable material could be produced using only the 2 MeV He^+ beam, which indicates that the RBS based alignment procedure can be used.

The pores produced in SiO_2, using this technique, had 15 nm larger pore diameter than the AAO mask used. This is attributed to the relatively low selectivity for the etching with 5% HF of irradiated and non-irradiated SiO_2. The selectivity is much higher for TiO_2, which will be discussed in the next section. The aspect-ratio for the study described here was about 2. Further studies have been made [84], where HF vapor etching was used instead. The results from those studies show that higher aspect-ratios could be obtained.

6.2 Pattern transfer to TiO_2

The AAO membranes used in this study were 2 μm in thickness with pore diameters of 70 nm and an inter-pore distance of ~100 nm. The same alignment procedure were used as in the case with the SiO_2 (see section 6.1). Instead of using chlorine ions, bromine ions were used. This ion beam was choosen because simulation showed that the Br^{7+} beam would be more appropriate for ion track formation in TiO_2. Three energies of the ion beam were used; 13, 25 and 32 MeV, all with a typical fluence of 8.0×10^{13} cm^{-2}.

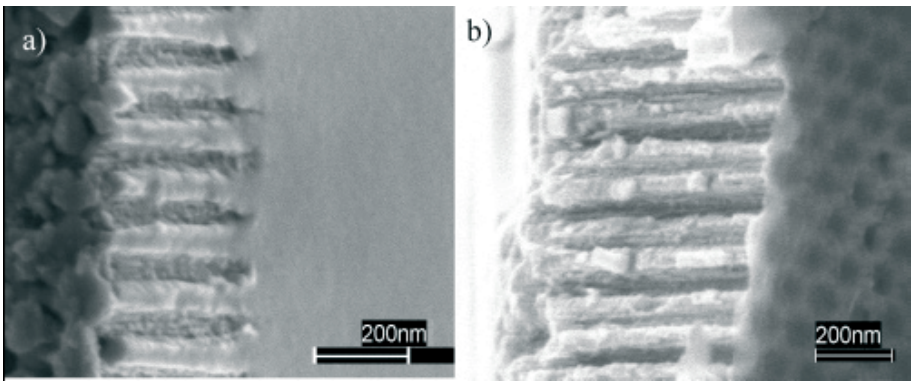

Figure 6.3. Cross sections tilted 30°; the average pore depth is (a) 600 nm (13 MeV Br^{7+} ions) and (b) 1100 nm (25 MeV Br^{7+} ions).

After irradiation and etching in HF, samples irradiated with 13 MeV Br^{7+} ions resulted in pores with depths of 600 nm (Figure 6.3 a), and the sample irradiated with 25 MeV Br^{7+} produced 1100 nm deep structures (Figure 6.3 b). In both cases the diameters of the pores on the irradiated samples correlates well with the pores in the AAO membranes used as mask, giving aspect-ratios of 9 and 16 on the two samples, respectively. When irradiating with a 32 MeV ion beam the threshold for etching is reached even under parts of the mask which not should be etched. This results in a non-ordered patterned surface and the role of the mask vanishes. An example of a larger patterned area is shown in Figure 6.4. It can be seen that the ordering from the mask is preserved through the irradiation and subsequent etching.

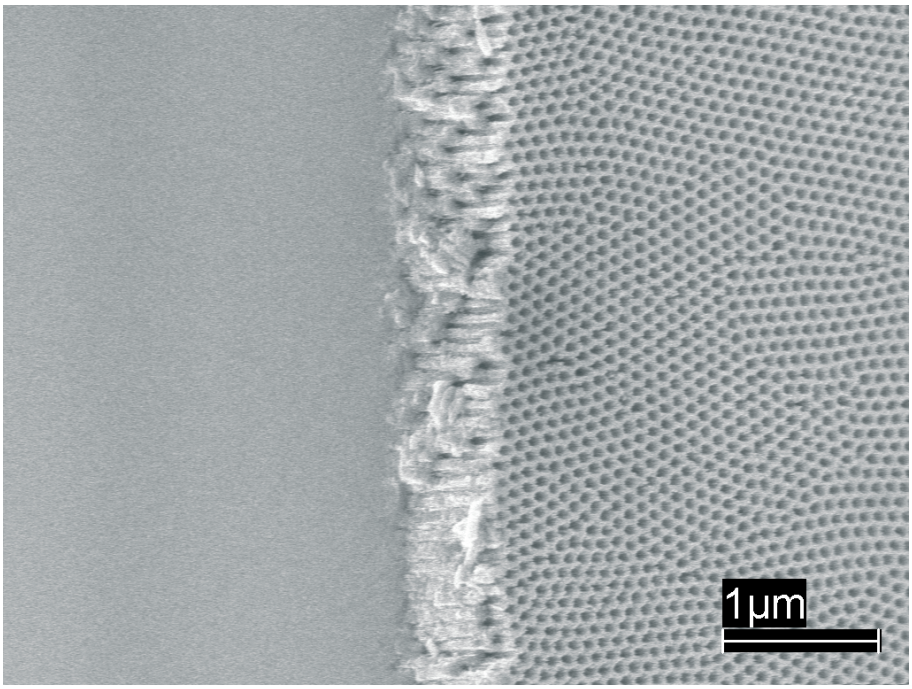

Figure 6.4. SEM image showing a TiO_2 surface to which the pattern from AAO have been transferred.

Simulations using SRIM200317 indicate that the depth of the pores should be 400 and 1680 nm for 13 and 25 MeV ion irradiation, respectively. When performing these simulations it is assumed that the alumina between the pores is perfectly dense. It has on the contrary been shown that the AAO membranes contain voids between the pores [85], and these voids do of course affect the density of the alumina.

7. Conclusions and future outlook

In the present thesis it has been demonstrated that the nanoporous membranes of anodic aluminium oxide have a large number of applications for fabrication of nanostructures. The AAO membrane can be manufactured in large quantities and there are numerous possibilities for tailoring the dimensions of the membrane well into the mezo-porous size range (2-50 nm). The thickness of the membrane can be monitored by changing the anodization time. The inter-pore distance as well as the pore diameters can be tailored by changing the anodization voltage. The degree of order of the pores can be determined by changing the anodization parameters, such as the electrolyte concentration and temperature. By exposing the fabricated AAO membranes to phosphoric acid the pores can be further widened (of course the pore diameter is limited by the inter-pore distance). After the anodization the membranes can be left on the aluminium substrate or the aluminium can be etched away in mercury chloride, depending on the application of the membrane.

There are numerous ways to fabricate nanoparticles, by wet-chemical techniques, by physical means in the gas phase *etcetera*. Two of the great challenges in the fabrications of nanoparticles are: 1. to get a narrow size distribution of the nanoparticles. 2. To get immobilized nanoparticles on different surfaces. In this thesis both these challenges were fulfilled for palladium nanoparticles, Prussian blue nanoparticles and for copper nanoparticles. All fabricated by different techniques and in all cases it was possible not only to get a narrow size distribution, but also to tailor the sizes in wide ranges. Pd and Prussian blue nanoparticles were fabricated through sequential electroless techniques, while copper nanoparticles were made through Atomic Layer Deposition (ALD).

The fabrication of monodisperse nanotubes are also described in this thesis. AAO membranes have been used as templates for deposition of Prussian blue nanotubes as well as niobium oxide nanotubes. The Prussian blue nanotubes were polycrystalline and fabricated using the same sequential techniques as was used with Prussian blue nanoparticles. The niobium oxide nanotubes were amorphous and fabricated using ALD. In both cases the outer diameter of the nanotubes were strictly restricted by the pore diameters of the AAO membrane used as template. The thicknesses of the tube walls could be tailored in both cases and by using a template which was well or-

dered with respect to the pores. The produced nanotubes could be arranged in a well ordered fashion as well.

By depositing nanoparticles or thin films of materials along the pore walls, the surface properties of the AAO membranes could be modified. If it is desirable to instead achieve other bulk properties, but still benefit from the well ordered pore arrangement, the pattern must be transferred to another material. Pattern transfer has been achieved using MeV ion beam lithography. AAO membranes were used as masks and heavy ions were irradiated through the masks onto an underlying substrate of another material. Prior to irradiation a careful alignment of the mask with respect to the ion beam were necessary. This was possible by a technique described in this thesis, which involves a gold marker layer and Rutherford backscattering spectroscopy (RBS). After alignment and irradiation it was possible to selectively etch in the regions of the underlying substrate which had been exposed to the highly energetic ion beam. The pattern from the AAO membranes were transferred to monocrystalline TiO_2 and amorphous SiO_2 substrates with good results. By using this technique it was possible to transfer the pattern of the AAO membranes to other materials on large areas (several mm^2, depending on the optics).

With the techniques described in this thesis individually or combining them with each other or other known techniques, it is possible to fabricate new nanomaterials. These new materials can be of use in a wide variety of application, such as in sensors and in the field of photo-cleavage of water. By depositing different thin films along the pore walls of AAO membranes interesting properties can be expected, which makes use of the large microscopic surface and the possibility to precisely tailor the properties of the thin films deposited. A first step is to deposit bi- and multilayered structures, and thereby produce multilayered nanotubes. These nanotubes can make use of properties from all the materials deposited and will surely have interesting properties and future applications.

8. Acknowledgements

First I want to express my deepest gratitude to my supervisor Professor Mats Boman. Professor Boman has been the best supervisor I ever could have imagined; his enthusiasm is not to be seen anywhere else.

I am also very grateful to my co-supervisor Professor Jan-Otto Carlsson, who gave me the opportunity to do my Ph D at Uppsala University.

All co-authors to the papers included in this thesis do also have my deepest gratitude. In the order they appear in the papers added to this thesis:

Dr. Alenka Razpet
Prof. Göran Possnert
Dr. Anders Hallén
Prof. Klas Hjort
Dr. Jun Lu
Ph. D. candidate Erika Widenkvist
Prof. Ulf Jansson
Dr. Tobias Törndahl
Dr. Mikael Ottosson
Ph. D. candidate Mårten Rooth
Prof. Anders Hårsta
Dr. Marek Skupinski
Ph. D. candidate Ruy Sanz
Dr. Jens Jensen
Prof. Manuel Vázquez

The co-authors I have worked with in other projects are also acknowledged. I want to thank all the people who have helped me at The Ångström Laboratory and especially at the Department of Materials Chemistry. The technical and administrative staff is acknowledged.

A special thanks is sent to those at the department who have made my non-working time pleasant.

Tack också till min fru Emma för att du liksom pallar med mig och har varit en grym hjälp under hela doktorandtiden. Tack till min familj och alla som faktiskt har trott på mig.

/Anders Johansson

9. Svensk sammanfattning

Nanoteknologi är ett område inom vetenskapen som fått otroligt mycket uppmärksamhet de senaste åren. I den här sammanfattningen tänkte jag lite kort beskriva vad nanoteknologi egentligen är och vad det är som gör den så spännande och viktig inför framtiden. Jag tänker också kort nämna min egen forskning och försöka ge en motivation till varför just den är viktig i framtida tillämpningar av nanotekniken.

Ordet ”nano” kommer från grekiskans ord för *dvärg*, och är ett måttenhetsprefix innebärande faktorn 10^{-9} (en miljarddel). En nanometer är således en miljarddels meter. Nanoteknologin är en teknologisk inriktning som ägnar sig åt att studera objekt som ligger i storleksintervallet 1 – 100 nm.

Varför är det då så intressant att studera objekt i denna ringa storlek? Börjar man fundera lite på vad det innebär att gå ner i storlek vid studier objekt så synsdet rätt snart att *ju mindre nanopartiklar är, ju större andel av atomerna sitter på ytan*. En partikel med en diameter på en nanometer har ungefär 90% av sina atomer på ytan, medan en partikel med en diameter på fem nanometer har ungefär 50% av sina atomer på ytan. Just det faktum att så många av atomerna sitter på ytan gör att nanoobjekt får väldigt speciella egenskaper. I vissa fall är de här ”nya egenskaperna” något som går att dra nytta av och försöka implementera i någon form av tillämpning; i andra fall är effekterna mer något som gör tillämpningar svårare. Jag tänkte börja med att ge tre praktiska exempel på när kunskaperna inom nanoteknologi måste börja användas.

En intressant tillämpning av nanoteknologin är inom sensortillverkningen. En spektroskopisk metod som är väldigt utbredd i är Ramanspektroskopin. Med hjälp av Ramanspektroskopi går det att med hög precision bestämma vad som finns i ett prov och också hur stora mängder som är närvarande av de olika ämnena. Problemet med Ramanspektroskopi är att det krävs rätt så höga halter av det som skall analyseras för att det analyserade ämnet skall uppräckas. För ett antal decenier sedan upptäckte forskare att nanopartiklar av guld och silver kan förstärka Ramansignalen så mycket som en miljon gånger. Innan analys utförs med Ramanspektroskopi kan provet exponeras för nanopartiklar av guld eller silver; på så vis kan signalen förstärkas med en faktor på upp till en miljon. Så pass mycket att det öppnar upp möjligheter för användningen av Ramanspektroskopi inom helt nya områden.

Elektroniska minnen är något som säljs i ofantliga kvantiteter idag. Vi vet alla att minnen minskar i storlek samtidigt som mer och mer data kan lagras i

dem. Ett elektroniskt minne är, enkelt uttryckt, något som kan lagra ettor och nollor. En etta kan vara en liten fläck i minnet som leder ström medan nollan inte leder ström. Ettan kan vara en punkt som är magnetiserad medan nollan inte är det. Det går också att tänka sig varianter där ettan har en viss färg medan nollan har en annan färg. Det viktiga är att det dels går att tillskriva en viss punkt på minnet en etta eller en nolla och att denna sedan kan läsas av på något sätt. Miniatyriseringen av elektroniska minnen förutsätter att vi kan göra just de här punkterna i minnet mindre och mindre, och där börjar faktiskt snart nanoteknologin göra intåg.

Ett bra exempel på när ”nanoeffekterna” är av ondo är inom elektronikindustrin. Vi vet alla att storleken på elektroniska komponenter minskar hela tiden. Ju mindre processorerna blir ju mer kraft kan tryckas in i dem på en mindre volym. När storleken på de individuella ledarna i en komponent börjar närma sig nanometersnivån börjar det hända lite underliga saker som t ex att elektronerna börjar smita. Detta är vad som händer när dimensionerna krymps för det vanligaste halvledarmaterialet som används idag, nämligen kiseloxid (SiO_2). Det går helt enkelt inte att bygga transistorer som är för små av kiseldioxid. För att kringgå problemet tittar man istället på nya material såsom hafniumoxid, titanoxid etc. Det räcker inte med att ta fram nya material till halvledarindustrin; det krävs också mycket kunskap i hur komponenterna skall tillverkas i nya material och det är just det en stor del av nanoteknologin handlar om.

Så hur tillverkas då objekt i nanometerstorlek? Kort sagt kan två huvudvägar följas:

1. *Top-down*. I vilket ett *bulkmaterial* används; detta bearbetas ner till nanometerstorlek med diverse fysikaliska metoder. Laserablation är ett vanligt exempel på detta. Även litografiska metoder används för att uppnå sådana resultat.
2. *Bottom-up*. Här är istället byggstenarna något på atomär och molekylär nivå; dessa byggstenar bygger upp nanomaterialet. Det är främst sådana tekniker som presenteras i den här avhandlingen.

I den här avhandlingen har vi utgått ifrån ett nanoporöst material för att tillverka andra nanostrukturer. Materialet som använts är anodiserad aluminiumoxid, som kan framställas på ett mycket välkontrollerat sätt; där finns möjlighet att bestämma porstorlek, graden av ordning mellan porerna, avståndet mellan porerna och tjockleken på membranet (se Figure 1.1). Detta porösa material används sedan på olika sätt för att tillverka andra nanostrukturerade material. Bland annat så belägger vi porväggarna med nanopartiklar av andra material såsom koppar, palladium och berlinerblått. Berlinerblått är ett blått pigment som varit känt i århundraden men som de senaste åren fått ökad uppmärksamhet då det har upptäckts att berlinerblått kan användas t ex för att rena vatten från radioaktivt cesium. Bland annat lät man renar få i sig

små mängder av berlinerblått efter Tjernobylolyckan. På detta vis kunde en hel del radioaktivt cesium drivas ut ur djuren. Berlinerblått har också ett stort antal besläktade ämnen med väldigt intressanta magnetiska egenskaper. Genom att belägga porväggarna i porös aluminiumoxid med koboltanalogen till berlinerblått så går det kanske i framtiden att tillverka extremt små elektroniska minnen med hög kapacitet.

Vi har också belagt porväggar med heltäckande material som nioboxid. Nioboxid är ett oxidmaterial som visat sig intressant i sensorsammanhang och också inom halvledarindustrin.

I vissa typer av tillämpningar kan det vara intressant att få ett helt annat material poröst på samma sätt som aluminiumoxiden. Dessvärre så är inte metoden för att tillverka porös aluminiumoxid tillämpbar på andra material; i alla fall inte på ett lika välkontrollerat sätt. Tidigare har jag beskrivet hur ytegenskaperna kan ändras hos den porösa aluminiumoxiden genom att deponering andra material på ytan, endera i form av nanopartiklar eller också i form av heltäckande tunna filmer. Är man däremot ute efter att erhålla porositet i ett annat material så måste man gå tillväga på andra sätt. I den här avhandlingen finns beskrivet hur det är möjligt att gå tillväga för att uppnå just sådana resultat. I korta drag handlar det om att en tunn ”mask” av just den porösa aluminiumoxiden placeras ovanpå ett annat material. Efter en rätt så komplicerad linjeringsprocedur så bestrålas sedan genom masken med joner med en väldigt hög hastighet och mycket energi. Jonerna går rakt igenom porerna i aluminiumoxiden och krockar sedan in i det underliggande materialet. I och med att jonerna har så hög energi som de har så skapas ”spår” i det underliggande materialet. Spåren skapas alltså bara direkt under masken där det varit hål och dessa spår går sedan att etsa upp med en syra som kallas för vätefluorid. På detta sätt har vi demonstrerat hur det är möjligt att föra över mönstret från porös aluminiumoxid till andra material, såsom kiseloxid och titanoxid.

Med den här avhandlingen har jag demonstrerat ett antal metoder för framställning av nanostrukturerade material. Alla material demonstrerade är i någon mån tillverkade i processer där porös aluminiumoxid har varit behjälplig, endera som schablon (templat), som poröst bärarmaterial eller som mask.

10. References

1. http://www.thebritishmuseum.ac.uk/science/lycurguscup/sr-lycugus-p1.html
2. G. Mie, Ann. Phys. 25, 377 (1908)
3. D. A. Weitz, T. J. Gramilla and A. Z. Genack, Phys. Rev. B. 22, 4562 (1980)
4. B. K. Russel, J. G. Mantovani, V. E. Anderson, R. J. Warmack and T. L. Ferrell, Phys. Rev. B. 35, 2151 (1987)
5. D. A. Bruggeman, Ann. Phys. (Leipzig) 24, 636 (1935)
6. J. C. Maxwell-Garnett, Philos. Trans. R. Soc. London 203, 385 (1904)
7. G. L. Hornyak, C. J. Patrissi, E. B. Oberhauser, C. R. Martin, J. –C. Valmalette, L. Lemaire, J. Dutta and H. Hofmann, Nanostr. Mater. 9, 571 (1997)
8. D. L. Feldheim and C. A. Foss, Jr. Metal Nanoparticles. Synthesis, Characterization and Applications (Marcel Dekker, New York, 2002)
9. D. Astruc, F. Lu and J. R. Aranzaes, Angew. Chem. Int. Ed. 44, 7852 (2005)
10. M. Fleischmann, P. J. Hendra and A J McQuillan, Chem. Phys. Lett. 26, 163 (1974)
11. A. Otto, Appl. Surf. Sci. 6, 309 (1980)
12. M. Muskovits, Rev. Mod. Phys. 57, 783 (1985)
13. G. Cao, Nanostructures & Nanomaterials: Synthesis, Properties & Applications, Imperial College Press, London, 2004
14. S. Iijima, Nature 354, 56 (1991)
15. M. Remškar, A. Mrzel, Vacuum 71, 177 (2003)
16. C. R. Martin, Science 266, 1961 (1994)
17. D. Routkevitch, T. Bigioni, M. Muskovits and J. M. Xu, J. Phys. Chem. 100, 14037 (1996)
18. K. Nielsch, F. Müller, A. P. Li and U. Gösele, Adv. Mater. 12, 582 (2000)
19. H. Masuda and K. Fukuda, Science 268, 1466 (1995)
20. G. E. Thompson, Thin Solid Films 297, 192 (1997)

21. A. P. Li, F. Müller, A. Birner, K. Nielsch and U. Gösele, J. Appl. Phys. 84, 6023 (1998)
22. O. Jessensky, F. Müller and U. Gösele, J. Electrochem. Soc. 145, 3735 (1998)
23. H. Masuda, H, Yamada, M. Satoh, H. Asoh, M. Nakao and T. Tamamura, Appl. Phys. Lett. 71, 2770 (1997)
24. C. Y. Liu, A. Datta, Y. L. Wang, Appl. Phys. Lett. 78, 120 (2001)
25. I. Mikulskas, S. Juodkazis, R. Tomasiumas, J. G. Dumas, Adv. Mater. 13, 1574 (2001)
26. S. Fournier-Bidoz, V. Kitaev, D. Routkevitch, I. Manners, G. A. Ozin, Adv. Mater. 16, 2193 (2004)
27. W. Lee, R. Li, C. A. Ross, U. Gösele and K. Nielsch, Small 2, 978 (2006)
28. W. Lee, R. Li, U. Gösele and K. Nielsch, Nat. Mater. 5, 741 (2006)
29. D. J. Sellmyer, M. Zheng and R. Skomski, J. Phys.: Condens. Matter 13, R433 (2001)
30. W. Lee, R. Scholz, K. Nielsch and U. Gösele, Angew. Chem. Int. Ed. 44, 6050 (2005)
31. L. Qu, G. Shi, X. Wu and B. Fan, Adv. Mater. 16, 1201 (2004)
32. M. Lahav, T. Sehayek, A. Vaskevich and I. Rubinstein, Angew. Chem. 42, 5576 (2003)
33. G. Schmid, J. Mater. Chem. 12, 1231 (2002)
34. T. Sawitowski, Y. Miquel, A. Heilmann and G. Schmid, Adv. Funct. Mater. 11, 435 (2001)
35. S. M. Marinakos, L. C. Brousseau, A. Jones and D. L. Feldheim, Chem. Mater. 10, 1214 (1998)
36. S. Vaucher, J. Fielden, M. Lei, E. Dujardin and S. Mann, Nano Lett. 2, 845 (2002)
37. P. H. Zhou and D. S. Xue, J. Appl. Phys. 96, 610 (2004)
38. K. Hashimoto, S. –I. Ohkoshi, Philos. Trans. R. Soc. London, Ser. A 357, 2977 (1999)
39. L. Catala, T. Gacoin, J. –P. Boilot, É. Rivière, C. Paulsen, E. Lhotel and T. Mallah, Adv. Mater. 15, 826 (2003)
40. S. –I. Ohkoshi, K. –I. Arai, Y. Sato and K. Hashimoto, Nat. Mater. 3, 857 (2004)
41. O. Sato, Y. Einaga, T. Iyoda, A. Fujishima and K. Hashimoto, J. Electrochem. Soc. 144, L11 (1997)

42. W. Jin, A. Toutianoush, M. Pyrasch, J. Schnepf, H. Gottschalk, W. Rammensee and B. Tieke, J. Phys. Chem. B 107, 12062 (2003)
43. M. Pyrasch, A. Tautianoush, W. Jin, J. Schnepf and B. Tieke, Chem. Mater. 15, 245 (2003)
44. A. Jaiswal, J. Colins, B. Agricole, P. Delhaes and S. Ravaine, J. Colloid Interface Sci. 261, 330 (2003)
45. S. Ravindran, K. V. Singh, G. T. S. Andavan, M. Ozkan, G. Yan, E. Hu and C. S. Ozkan, Nanotechnology 17, 714 (2006)
46. T. Suntola and J. Antson, US Patent no. 4,058,430: Method for Producing Compound Thin Films, (1977)
47. P. Mårtensson and J. –O. Carlsson, Chem. Vap. Deposition 3, 45 (1997)
48. B. S. Lim, A. Rahtu and R. Gordon, Nat. Mater. 2, 749 (2003)
49. T. Törndahl, M. Ottosson and J. –O. Carlsson, Thin Solid Films 458, 129 (2004)
50. T. Törndahl, M. Ottosson and J. –O. Carlsson, J. Electrochem. Soc. 153, C146 (2006)
51. R. L. Puuranen, J. Appl. Phys. 97, 121301 (2005)
52. J. –O. Carlsson, Thin Solid Films 130, 261 (1985)
53. K. Kukli, M. Ritala, M. Leskelä and R. Lappalainen, Chem. Vap. Deposition 4, 29 (2002)
54. A. Hårsta, J. Phys. IV France 11, Pr3 (2001)
55. M. Schuisky, Thesis, Acta Univ. Ups. (Fac. Sci.) 594 (2000)
56. K. Forsgren, Thesis, Acta Univ. Ups. (Fac. Sci.) 665 (2001)
57. J. Sundqvist, Thesis, Acta Univ. Ups. (Fac. Sci.) 852 (2003)
58. M. Rooth, K. Kukli and A. Hårsta, in EUROCVD 15, Proc. Vol. 2005-09, Eds.: A. Devi, R. Fisher, H. Parala, M. Allendorf and M. Hitchman (The Electrochem. Soc., Pennington, N. J. 2005) p. 598
59. J. W. Elam, D. Routkevitch, P. P. Mardilovich and S. M. George, Chem. Mater. 15, 3507 (2003)
60. G. Xiong, J. W. Elam, H. Feng, C. Y. Han, H. -H. Wang, L. E. Iton, L. A. Curtiss, M. J. Pellin, M. Kung, H. Kung and P. C. Stair, J. Phys, Chem. B 109, 14059 (2005)
61. K. Hjort, G. Thornell, R. Spohr and J. –Å. Schweitz, Appl. Phys. Lett. 69, 3435 (1996)
62. M. Lindeberg and K. Hjort, Sens. Actuators, A 105, 150 (2003)

63. M. Toulemonde, C. Trautmann, E, Balanzat, K. Hjort and A. Weidinger, Nucl. Instrum. Methods Phys. Res. B 216, 1, (2004)
64. D. Almawlawi, K. A. Bosnick, A. Osika and M. Moskovits, Adv. Mater. 12, 1252 (2000)
65. N. Matsuura, T. W. Simpson, I. V. Mitchell, X. –Y. Mei, P. Morales and H. E. Ruda, Appl. Phys. Lett. 81, 4826 (2002)
66. L. E. Rehn, B. J. Kestel, P. M. Baldo, J. Hiller, A. W. McCormick and R. C. Birtcher, Nucl. Instrum. Methods Phys. Res. B 206, 490 (2003)
67. C. Jamois, L. C. Wehrspohn, R. B. Andreani, C. Hermann, O. Hess and U. Gösele, Photonics and Nanostructures: Fundamentals and Applications 1, 1 (2003)
68. H. Asoh, M. Matsuo, M. Yoshihama and S. Ono, Appl. Phys. Lett. 83, 4408 (2003)
69. U. Diebold, Surf. Sci. Rep. 48, 53 (2003)
70. G. K. Mor, K. Shankar, M. Paulose, O. K. Varghese and C. A. Grimes, Nano Lett. 5, 191 (2003)
71. W. W. Walker, Microstruct. Sci. 7, 287 (1979)
72. P. Steinmetz, S. Alperine, A. Friant- Constantini and P. Rosso, Surf. Coat. Technol. 43/44, 500 (1990)
73. K. Kordás, J. Békési, R. Vajtai, L. Nánai, S. Leppävuori, A. Uusimäki, K. Bali, T. F. George, G. Galbács, F. Ignácz and P. Moilanen, Appl. Surf. Sci. 172, 178 (2001)
74. L. B. Kiss, J. Söderlund, G. A. Niklasson and C. –G. Granqvist, Nanotechnology 10, 25 (1998)
75. J. Reid, Jpn. J. Appl. Phys. 40, 2650 (2001)
76. Y. Shacham-Diamand, V. Dubin and M. Angyal, Thin Solid Films 262, 93 (1995)
77. J. –Y. Kim, Y. –K. Lee, H. –S. Park, J. –W. Park, D. –K. Park, J. –H. Joo, W. –H. Lee, Y. –K. Ko, P. J. Reucroft and B. –R. Cho, Thin Solid Films 330, 190 (1998)
78. A. V. Gelatos, R. Marsh, M. Kottke and C. J. Mogab, Appl. Phys. Lett. 63, 2842 (1993)
79. A. Jain, K. –M. Chi, T. T. Kodas, M. J. Hampden-Smith, J. D. Farr and M. F. Paffett, Chem. Mater. 3, 995 (1991)
80. G. Riveros, H. Gómez, A. Cortes, R. E. Marotti and E. A. Dalchiele, Appl. Phys. A 81, 17 (2005)
81. Z. Li, R. G. Gordon, D. B. Farmer, Y. Lin and J. Vlassak, Electrochem. Solid. St. 8, G182 (2005)

82. J. Sundqvist, A. Hårsta, J. Aarik, K. Kukli and A. Aidla, Thin Solid Films 427, 147 (2003)
83. K. Awazu, S. Ishii, K. Shima, S. Roorda and J. L. Brebner, Phys. Rev. B 62, 3689 (2000)
84. M. Skupinski, Thesis, Acta Univ. Ups. (Fac. Sci.) 229 (2006)
85. Y. F. Mei, X. L. Wua, X. F. Shaoa, G. S. Huanga and G. G. Siub, Phys. Lett. A 309, 109 (2003)

Acta Universitatis Upsaliensis

Digital Comprehensive Summaries of Uppsala Dissertations from the Faculty of Science and Technology 246

Editor: The Dean of the Faculty of Science and Technology

A doctoral dissertation from the Faculty of Science and Technology, Uppsala University, is usually a summary of a number of papers. A few copies of the complete dissertation are kept at major Swedish research libraries, while the summary alone is distributed internationally through the series Digital Comprehensive Summaries of Uppsala Dissertations from the Faculty of Science and Technology. (Prior to January, 2005, the series was published under the title "Comprehensive Summaries of Uppsala Dissertations from the Faculty of Science and Technology".)

Distribution: publications.uu.se
urn:nbn:se:uu:diva-7364

ACTA
UNIVERSITATIS
UPSALIENSIS
UPPSALA
2006